The Astrophysical Journal Supplement Series, 196:21 (18pp), 2011 October doi:10.1088/0067-0049/196/2/21

A MULTI-EPOCH, SIMULTANEOUS WATER AND METHANOL MASER SURVEY TOWARD INTERMEDIATE-MASS YOUNG STELLAR OBJECTS

Jae-Han Bae[1], Kee-Tae Kim[1], So-Young Youn[1], Won-Ju Kim[1,2], Do-Young Byun[1], Hyunwoo Kang[1,3], and Chung Sik Oh[1]
[1] Korea Astronomy and Space Science Institute, Hwaam-Dong, Yuseong-Gu, Daejeon 305-348, Korea; jaehbae@umich.edu, whorujh@kasi.re.kr, ktkim@kasi.re.kr
[2] Department of Astronomy and Space Science, Chungnam National University, Daejeon 305-764, Korea
[3] Department of Physics and Astronomy, FPRD, Seoul National University, Seoul 151-742, Korea
Received 2011 February 24; accepted 2011 August 17; published 2011 September 30

ABSTRACT

We report a multi-epoch, simultaneous 22 GHz H_2O and 44 GHz Class I CH_3OH maser line survey toward 180 intermediate-mass young stellar objects, including 14 Class 0 and 19 Class I objects, and 147 Herbig Ae/Be stars. We detected H_2O and CH_3OH maser emission toward 16 (9%) and 10 (6%) sources with one new H_2O and six new CH_3OH maser sources. The detection rates of both masers rapidly decrease as the central (proto)stars evolve, which is contrary to the trends in high-mass star-forming regions. This suggests that the excitations of the two masers are closely related to the evolutionary stage of the central (proto)stars and the circumstellar environments. H_2O maser velocities deviate on average 9 km s^{-1} from the ambient gas velocities whereas CH_3OH maser velocities match quite well with the ambient gas velocities. For both maser emissions, large velocity differences ($|v_{H_2O} - v_{sys}| > 10$ km s^{-1} and $|v_{CH_3OH} - v_{sys}| > 1$ km s^{-1}) are mostly confined to Class 0 objects. The formation and disappearance of H_2O masers is frequent and their integrated intensities change by up to two orders of magnitude. In contrast, CH_3OH maser lines usually show no significant change in intensity, shape, or velocity. This is consistent with the previous suggestion that H_2O maser emission originates from the base of an outflow while 44 GHz Class I CH_3OH maser emission arises from the interaction region of the outflow with the ambient gas. The isotropic maser luminosities are well correlated with the bolometric luminosities of the central objects. The fitted relations are $L_{H_2O} = 1.71 \times 10^{-9} (L_{bol})^{0.97}$ and $L_{CH_3OH} = 1.71 \times 10^{-10} (L_{bol})^{1.22}$.

Key words: ISM: molecules – masers – stars: formation – stars: pre-main sequence – stars: protostars

Online-only material: color figure

1. INTRODUCTION

Maser emission is an important signpost of star formation, especially at the early stages. Since the discovery of the first maser line, the OH emission at a frequency of 1665 MHz by Weaver et al. (1965), many surveys have been performed toward star-forming regions at various frequencies, e.g., 1.66540 GHz and 1.66736 GHz (OH maser lines), 6.66852 GHz (Class II CH_3OH $5_1 - 6_0 A^+$ maser line), 22.23508 GHz (H_2O $6_{16} - 5_{23}$ maser line), 42.82059 GHz and 43.12208 GHz (SiO $v = 1, 2$, $J = 1-0$ maser lines), and 44.06943 GHz (Class I CH_3OH $7_0 - 6_1 A^+$ maser line).

22 GHz H_2O masers are thought to be pumped by the excitation of the H_2O rotation states in collisions with H_2 molecules (Elitzur et al. 1989). Previous surveys of H_2O masers have shown that this maser is frequently observed toward young stellar objects (YSOs) over a wide range of masses (Genzel & Downes 1977; Rodriguez et al. 1980) and exhibits a wide range of relative velocities with respect to the parental dense cores (Felli et al. 1992; Furuya et al. 2005; Breen et al. 2010; Caswell & Breen 2010). High-resolution studies of the individual YSOs have revealed that H_2O masers are located very close ($\lesssim$1000 AU) to the central (proto)stars (Claussen et al. 1998; Martí et al. 1999; Seth et al. 2002; Furuya et al. 2005).

CH_3OH masers are the most recent maser species to be intensively studied. There are numerous transitions that can be divided into two classes, I and II, according to the classification of Menten (1991). Class I CH_3OH maser transitions include the $4_{-1} - 3_0 E$, $7_0 - 6_1 A^+$, $5_{-1} - 4_0 E$, and $8_0 - 7_1 A^+$ lines at 36, 44, 84, and 95 GHz, while Class II CH_3OH maser transitions include the $5_1 - 6_0 A^+$, $2_0 - 3_{-1} E$, and $J_0 - J_{-1} E$ lines at 6.7, 12, and 157 GHz. Even though both classes are commonly observed in (high-mass) star-forming regions, their pumping mechanisms are known to be different. Using theoretical models, Cragg et al. (1992) suggested that Class I CH_3OH masers result from collisional excitation, while Class II CH_3OH masers appear when there is a source of continuum radiation.

The CH_3OH maser at 44 GHz is the most common and strongest Class I maser. Nevertheless, only ~200 sources have been detected until now (Val'tts et al. 2010). 44 GHz Class I CH_3OH masers are thought to be associated mainly with high-mass star formation, yet interferometric observations found that they are usually offset by ~0.1–1 pc from other signposts of star formation, such as ultracompact H II (UCHII) regions, infrared sources, and H_2O masers (Kurtz et al. 2004; Cyganowski et al. 2009). The observed 44 GHz CH_3OH maser velocities are different from the ambient molecular gas velocities by $\lesssim$10 km s^{-1} (Bachiller et al. 1990; Fontani et al. 2010), which is much smaller compared to H_2O maser relative velocities.

Intermediate-mass stars have masses of 2–10 $M_\odot$. These lower and upper boundaries are of importance. First, pre-main sequence (PMS) stars with masses >2 $M_\odot$ are expected to follow fully radiative tracks once the quasi-static contraction has ended (Waters & Waelkens 1998). This implies that these stars could evolve in different ways from lower-mass stars. Second, stars more massive than ~10 $M_\odot$ spend their whole PMS stage as obscured objects (Waters & Waelkens 1998), which means that they are not visible until they reach the main sequence. Intermediate-mass YSOs (IMYSOs) share many characteristics with their high-mass counterparts, but many of them are

located far closer to the Sun and are less deeply embedded (Alonso-Albi et al. 2009). Thus, it would be helpful to study IMYSOs to understand high-mass star formation.

Despite the importance of studying IMYSOs, no systematic maser line surveys toward them have been undertaken so far. Maser observations toward IMYSOs were usually made as part of surveys targeting low-mass YSOs (e.g., Claussen et al. 1996; Furuya et al. 2003). Otherwise, maser surveys have been limited to Herbig Ae/Be (HAeBe) stars (e.g., Palla & Prusti 1993), which are recognized as intermediate-mass PMS stars (see Thé et al. 1994 and references therein): have spectral types of A or earlier, with emission lines; lie in an obscured region; and illuminate fairly bright nebulosity in their immediate vicinity.

In this study, we present a multi-epoch, simultaneous H_2O and 44 GHz Class I CH_3OH maser line survey toward 180 IMYSOs in various evolutionary stages. This paper is organized as follows. The source selection and the observations are described in Sections 2 and 3, respectively. We present the results with some comments on the individual sources in Section 4 and discuss the observational results in Section 5. We summarize the main results in Section 6.

2. SOURCE SELECTION

To define our sample of IMYSOs, we collected sources from published studies satisfying one of the following two criteria: (1) protostellar or PMS objects with bolometric luminosities of $40\,L_\odot < L_{\rm bol} \lesssim 1000\,L_\odot$, which are thought to be the precursors of intermediate-mass stars; or (2) known or candidate HAeBe stars. All selected sources have declinations greater than -30°.

We first selected objects that satisfy criterion (1): 14 Class I objects from Saraceno et al. (1996); 4 Class 0, 3 Class 0/I, 5 Class I, 1 HAeBe, and 9 unclassified sources from Furuya et al. (2003); 4 Class 0, 5 Class 0/I, 4 Class I, and 1 unclassified source from Froebrich (2005); 7 Class 0 and 2 Class I objects from Alonso-Albi et al. (2010). To clarify the evolutionary stages of the collected unclassified objects, we consulted additional classification works, which are noted in Column 5 of Table 1. Considering the overlapped sources from the references mentioned above, we produced a sample containing 14 Class 0, 19 Class I, and 2 HAeBe objects from the first criterion.

We then collected objects satisfying criterion (2). They are primarily selected from catalogs published by Thé et al. (1994) and Vieira et al. (2003). Thé et al. (1994) presented 108 Be and Ae stars, which were historically recognized as true members or potential candidates of the HAeBe stellar group, and Vieira et al. (2003) suggested 131 HAeBe stars and candidates. Of members in the two catalogs, 86 sources in Thé et al. (1994) and 76 sources in Vieira et al. (2003) are north of -30° with 22 sources in common. Our sample also contains five other HAeBe stars: BD+24°676, BD+41°3731, V517 Cyg, and V1057 Cyg from Palla & Prusti (1993), and V1318 CygS from Palla et al. (1995). Thus, the complete sample satisfying the second criterion would be 145 HAeBe stars.

In summary, our sample consists of 180 IMYSOs: 14 Class 0, 19 Class I, and 147 HAeBe stars. The objects in our sample are listed in Table 1.

3. OBSERVATIONS

We carried out a multi-epoch, simultaneous survey of H_2O $6_{16} - 5_{23}$ (22.23508 GHz) and Class I CH_3OH $7_0 - 6_1 A^+$ (44.06943 GHz) maser lines toward 180 IMYSOs. The observations were performed using the Korean Very Long Baseline Interferometry Network (KVN) 21 m radio telescope at the Yonsei station over three different periods. The first observations were conducted toward all of the 180 IMYSO samples during 21 days from 2010 January to May. On 2010 October 20 and December 2, the second and third epochs were observed toward the 26 objects that showed maser emission in the first epoch.

The telescope is equipped with a multi-frequency receiving system, which makes it possible to observe at both frequencies simultaneously (Han et al. 2008). The 86 GHz and 129 GHz receivers will be added to the receiving system in 2011 for simultaneous observations in four different frequency bands. We used 4096 channel Digital Spectrometers, each with 32 MHz bandwidth. Table 2 presents a summary of the observations.

The pointing and focus checks were made every 2 hr using nearby known strong H_2O maser sources. The pointing accuracy was maintained to better than 5″ during the observations. The data were calibrated by the standard chopper wheel method and the line intensity was obtained on the T_A^* scale. The conversion factors between T_A^* and the flux density are 11.1 Jy K^{-1} at 22 GHz and 11.6 Jy K^{-1} at 44 GHz.

All the observations were made using position switching mode with total (ON+OFF) integration time of 30 minutes, which typically yields about 0.5 Jy rms noise levels for both maser transitions at 0.21 km s^{-1} velocity resolution. Since the KVN telescopes are of the shaped Cassegrain type, they have a smaller full width at half-maximum (FWHM) primary beam and much higher (∼14 dB) first sidelobe levels than conventional Cassegrain antennas with the same size primary reflectors (Kim et al. 2011; Lee et al. 2011). The first sidelobes are separated by about 1.5 times the FWHM from the primary beam center. To determine whether the detected maser emission is contaminated by nearby bright maser sources, we mapped an area of 1.5 FWHM × 1.5 FWHM around each source with detectable maser emission using half-beam spacing. All data were reduced with the CLASS software.

4. RESULTS

4.1. Overall Results

Of the 180 IMYSOs observed, we detected H_2O and CH_3OH maser emission toward 20 and 12 sources, respectively (Figures 1 and 2). All the detected maser lines are limited to signals stronger than the 3σ rms noise level. However, several objects are located close enough to one another that they fall within a single beam or its sidelobes. Further analysis shows that four H_2O and two CH_3OH masers do not arise from the target IMYSOs. Those sources will be discussed in detail below. In total, 16 sources show H_2O maser emission and 10 sources show CH_3OH maser emission. Six objects emit both H_2O and CH_3OH maser emission. Consequently, the detection rates of H_2O masers and CH_3OH masers are 9% (16/180) and 6% (10/180), respectively. One intriguing source is IRAS 20050+2720 MMS1, which shows extremely blueshifted (∼−90 km s^{-1}) H_2O maser line emission with respect to the molecular gas. Furuya et al. (2003) suggested that this emission might be related to an extremely high-velocity CO outflow emanating from the central protostar (Bachiller et al. 1995). The observed properties of all detected H_2O and CH_3OH maser lines are presented in Tables 3 and 4: the source name in Column 1, the observing date in Column 2, the Gaussian-fitted line flux, peak velocity, and line width (FWHM) in

Table 1
Source Summary

Source	R.A.	Decl.	Source Type[a]	Ref.	Distance	Ref.	L_{bol}	Ref.	Observing	Detection		σ_{H_2O}	σ_{CH_3OH}
	(J2000)	(J2000)			(pc)		($L_\odot$)		Date	H_2O	CH_3OH	(Jy)	(Jy)
(1)	(2)	(3)	(4)	(5)	(6)	(7)	(8)	(9)	(10)	(11)	(12)	(13)	(14)
MacC H12	00 07 02.6	+65 38 38	HAeBe(?)	1, 2	845	3	47.1	3	2010 Feb 24	N	N	0.46	0.52
HBC 324	00 07 30.7	+65 39 52	HAeBe	1, 2	850	4	60	4	2010 Mar 18	N	N	0.36	0.47
LkHα 198	00 11 26.0	+58 49 29	HAeBe	1, 2	600	4	115	4	2010 Feb 24	N	N	0.46	0.55
V376 Cas	00 11 26.1	+58 50 04	HAeBe(?)	1, 2	630	5	437	5	2010 Feb 24	N	N	0.49	0.51
CB 3	00 28 42.7	+56 42 07	Class 0	6	2500	6	1000	6	2010 May 8	Y	Y[b]	0.45	0.53
VX Cas	00 31 30.7	+61 58 51	HAeBe	1, 2	619	7	31	7	2010 Feb 24	N	N	0.43	0.46
IRAS 00338+6312	00 36 47.5	+63 29 02	Class I	8	850	8	1100	8	2010 Jan 18	Y	Y[b]	0.32	0.41
V594 Cas	00 43 18.3	+61 54 40	HAeBe(?)	1, 2	650	5	1950	5	2010 Mar 18	N	N	0.36	0.48
RNO 6	02 16 30.1	+55 22 57	HAeBe	1, 2	1600	4	562	4	2010 Mar 18	N	N	0.36	0.51
NGC1333 IRAS2[c]	03 28 56.3	+31 14 34	Class 0	8, 9	220	8	43	9	2010 May 8	N	N	0.49	0.51
NGC1333 SVS 13A	03 29 03.8	+31 16 04	Class 0	8, 10	220	8	47	10	2010 May 9	N	N	0.54	0.59
IRAS 03359+2932	03 39 00.6	+29 41 46	HAeBe	11, 12	...	...	...	...	2010 Feb 24	N	N	0.45	0.46
IP Per	03 40 47.0	+32 31 54	HAeBe	1, 2	350	5	14	5	2010 Feb 24	N	N	0.45	0.47
XY Per e+w	03 49 36.3	+38 58 55	HAeBe	1, 2	347	7	86	7	2010 Mar 18	N	N	0.48	0.51
V892 Tau	04 18 40.6	+28 19 16	HAeBe	1, 2	160	5	2239	5	2010 Mar 17	N	N	0.36	0.56
IRAS 04278+2253	04 30 50.3	+23 00 09	HAeBe	11	...	...	...	...	2010 Feb 24	N	N	0.47	0.47
BD+24°676	04 40 32.6	+24 26 31	HAeBe	13	...	...	...	...	2010 Apr 19	N	N	0.71	0.78
AB Aur	04 55 45.8	+30 33 04	HAeBe	1, 2, 11	144	5	69	5	2010 Mar 19	N	N	0.38	0.40
MWC 480	04 58 46.3	+29 50 37	HAeBe	1, 11, 12	146	7	22	7	2010 Feb 24	N	N	0.45	0.47
UX Ori	05 04 30.0	−03 47 14	HAeBe	1, 2	517	7	37	7	2010 Mar 18	N	N	0.43	0.63
IRAS 05044−0325	05 06 55.5	−03 21 13	HAeBe(?)	11, 12, 14	...	...	670	15	2010 Mar 18	N	N	0.39	0.59
V1012 Ori	05 11 36.5	−02 22 48	HAeBe	1	...	...	...	...	2010 Mar 18	N	N	0.34	0.51
V1366 Ori	05 16 00.5	−09 48 35	HAeBe	1, 11, 12	164	5	5	5	2010 Mar 21	N	N	0.42	0.56
IRAS 05209+2454	05 24 01.2	+24 57 38	HAeBe	11	150	5	23	5	2010 Feb 24	N	N	0.49	0.51
IRAS 05215+0225	05 24 08.0	+02 27 47	HAeBe	11, 12	...	...	...	...	2010 Mar 17	N	N	0.48	0.56
V346 Ori	05 24 42.8	+01 43 48	HAeBe	1, 11, 12	586	7	61	7	2010 Mar 21	N	N	0.39	0.53
IRAS 05245+0022	05 27 05.5	+00 25 08	HAeBe	11, 12	...	...	...	...	2010 Mar 17	N	N	0.47	0.58
HD 35929	05 27 42.8	−08 19 38	HAeBe	1, 16	345	5	79	5	2010 Mar 18	N	N	0.37	0.55
IRAS F05272−0025	05 29 48.0	−00 23 43	HAeBe	11	...	...	...	...	2010 Mar 18	N	N	0.36	0.52
IRAS 05275+1118	05 30 19.0	+11 20 20	HAeBe	11, 12	...	...	...	...	2010 Mar 18	N	N	0.34	0.51
MWC 758	05 30 27.5	+25 19 57	HAeBe	1, 11, 12	205	5	28	5	2010 Feb 24	N	N	0.64	0.56
HK Ori	05 31 28.1	+12 09 10	HAeBe(?)	1, 2	460	5	78	5	2010 Mar 17	N	N	0.39	0.61
V1410 Ori	05 31 57.2	+11 17 41	HAeBe	1, 16	336	5	98	5	2010 Mar 19	N	N	0.37	0.56
IRAS 05295−0458	05 32 00.3	−04 55 54	HAeBe	11	...	...	...	...	2010 Mar 24	N	N	0.32	0.35
IRAS 05293+1701	05 32 14.1	+17 03 29	HAeBe(?)	11, 12	...	...	...	...	2010 Feb 24	N	N	0.64	0.59
IRAS 05302−0537	05 32 41.7	−05 35 48	Class I	8	450	8	40	8	2010 Jan 14	N	N	0.72	0.56
HD 245185	05 35 09.6	+10 01 52	HAeBe	1, 2	400	5	22	5	2010 Mar 19	N	N	0.67	0.71
OMC3 MMS6[d]	05 35 23.5	−05 01 32	Class 0	8, 11	450	8	<100	9	2010 May 8	N	N	0.62	0.46
OMC3 MMS9[d]	05 35 26.0	−05 05 42	Class I	8, 11	450	8	130	9	2010 May 8	N	Y[b]	0.66	0.69
OMC3 MMS7[d]	05 35 26.6	−05 03 56	Class I	9	450	8	53	9	2010 May 8	N	N	0.72	0.63
OMC2 FIR4[d]	05 35 27.0	−05 10 06	Class 0	6	450	8	1000	6	2010 May 6	N	Y	0.66	0.69
T Ori[d]	05 35 50.4	−05 28 35	HAeBe	1, 2	472	7	50	7	2010 Mar 17	N	N	0.49	0.59
IRAS 05335−0645	05 35 57.0	−06 43 41	Class I	17	480	15	52	17	2010 May 7	N	N	0.55	0.63
CQ Tau	05 35 58.5	+24 44 54	HAeBe	1, 2	100	5	3.5	5	2010 Mar 17	N	N	0.42	0.68
IRAS 05338−0624	05 36 17.6	−06 22 10	Class I	8, 18	480	8	144	8	2010 Jan 13	Y	Y[b]	0.36	0.51
IRAS 05338−0647	05 36 18.2	−06 45 47	Class I	8, 19	440	8	70	8	2010 May 8	Y	N	0.67	0.67
HH147 MMS	05 36 25.1	−06 44 42	Class I	9, 17	460	20	45	17	2010 May 8	N	N	0.58	0.61
V380 Ori	05 36 25.4	−06 42 58	HAeBe(?)	1, 2	510	5	933	5	2010 Mar 21	N	N	0.36	0.45
IRAS 05339−0626	05 36 25.5	−06 25 02	Class I	17	500	21	59	17	2010 May 8	N	N	0.56	0.62
IRAS 05342−0639	05 36 40.6	−06 38 03	Class I	17	...	...	48	17	2010 May 8	N	N	0.56	0.59
V586 Ori	05 36 59.3	−06 09 16	HAeBe	1, 16	510	5	87	5	2010 Mar 24	N	N	0.48	0.53
IRAS 05345−0139	05 37 02.4	−01 37 21	HAeBe	11	...	...	...	...	2010 Mar 23	N	N	0.44	0.59
BF Ori	05 37 13.3	−06 35 01	HAeBe(?)	1, 2	603	7	62	7	2010 Mar 24	N	N	0.54	0.61
KMS 27	05 37 47.1	+06 42 30	HAeBe	1, 11, 12	...	...	...	...	2010 Mar 24	N	N	0.54	0.63
IRAS 05355−0117	05 38 05.2	−01 15 22	HAeBe	11, 12	...	...	...	...	2010 Mar 24	N	N	0.62	0.68
V1787 Ori	05 38 09.2	−06 49 16	HAeBe	1, 11	...	...	...	...	2010 Mar 24	N	N	0.43	0.59
V1788 Ori	05 38 14.5	−05 25 13	HAeBe	1, 11, 12	...	...	...	...	2010 Mar 23	N	N	0.44	0.56
Haro 13a	05 38 18.2	−07 02 26	HAeBe	1	...	...	...	...	2010 Mar 24	N	N	0.48	0.52
V599 Ori	05 38 58.6	−07 16 46	HAeBe	1, 11	360	15	...	...	2010 Mar 16	N	N	0.38	0.58
ω Ori	05 39 11.1	+04 07 17	HAeBe	1	...	...	...	...	2010 Mar 16	N	N	0.37	0.58
RR Tau	05 39 30.5	+26 22 27	HAeBe	1, 2	2103	7	781	7	2010 Mar 16	N	N	0.34	0.53
IRAS 05375−0731	05 39 56.1	−07 30 26	Class 0	6	500	6	67	6	2010 Jan 18	Y	N	0.39	0.53
V350 Ori	05 40 11.8	−09 42 11	HAeBe	1, 2	735	7	29	7	2010 Mar 16	N	N	0.39	0.58
Reipurth50 NIRS1	05 40 27.7	−07 27 28	Class I	17	...	...	212	17	2010 May 9	N	N	0.59	0.58

Table 1
(Continued)

Source	R.A.	Decl.	Source Type[a]	Ref.	Distance	Ref.	L_{bol}	Ref.	Observing	Detection		σ_{H_2O}	σ_{CH_3OH}
	(J2000)	(J2000)			(pc)		($L_\odot$)		Date	H_2O	CH_3OH	(Jy)	(Jy)
(1)	(2)	(3)	(4)	(5)	(6)	(7)	(8)	(9)	(10)	(11)	(12)	(13)	(14)
MWC 120	05 41 02.3	−02 43 01	HAeBe	1, 16	470	5	138	5	2010 Mar 24	N	N	0.48	0.53
NGC 2023 MM 1	05 41 24.9	−02 18 09	Class 0	22	730	15	200	17	2010 May 9	N	N	0.64	0.61
IRAS 05407−0501	05 43 11.9	−04 59 50	HAeBe	11, 12	460	5	123	5	2010 Mar 21	N	N	0.39	0.56
IRAS 05417+0007	05 44 18.8	+00 08 40	HAeBe	11, 12	...	...	...	...	2010 Mar 23	N	N	0.47	0.62
IRAS 05451+0037	05 47 42.3	+00 38 40	Class I	8	450	8	40	8	2010 Jan 18	N	N	0.42	0.58
IRAS 05471+2351	05 50 13.5	+23 52 17	HAeBe(?)	11, 12, 14	...	...	...	...	2010 Mar 19	N	N	0.52	0.47
IRAS 05513−1024	05 53 42.6	−10 24 01	HAeBe	11, 11	470	23	5.1	23	2010 Mar 16	N	N	0.38	0.59
IRAS 05555−1405	05 57 49.5	+14 05 34	HAeBe	11	470	23	4.8	23	2010 Mar 21	N	N	0.44	0.56
IRAS 05560+1639	05 58 55.6	+16 39 58	HAeBe	11, 12	...	...	...	...	2010 Mar 21	N	N	0.44	0.55
HD 250550	06 02 00.0	+16 30 57	HAeBe	1, 2	700	5	275	5	2010 Mar 16	N	N	0.37	0.49
IRAS 05598−1000	06 02 14.9	−10 01 00	HAeBe	11, 12	...	...	...	...	2010 Mar 18	N	N	0.37	0.56
IRAS 06013−1452	06 03 37.1	−14 53 03	HAeBe	11, 12	...	...	...	...	2010 Mar 16	N	N	0.43	0.56
IRAS 06045−0554	06 06 58.5	−05 55 08	HAeBe	11, 12	...	...	...	...	2010 Mar 24	N	N	0.54	0.58
IRAS 06040+2958	06 07 16.1	+29 58 01	HAeBe	11	...	...	...	...	2010 Mar 19	N	N	0.54	0.49
LkHα 208	06 07 49.5	+18 38 26	HAeBe	1, 2	1000	5	85	5	2010 Mar 19	N	N	0.54	0.51
IRAS 06071+2925	06 10 17.5	+29 25 16	HAeBe	11	...	...	...	...	2010 Mar 19	N	N	0.54	0.46
LkHα 339	06 10 57.8	−06 14 37	HAeBe	1, 2	830	5	105	5	2010 Mar 23	N	N	0.43	0.61
IRAS 06111−0624	06 13 36.2	−06 25 02	HAeBe	11, 12	...	...	...	...	2010 Mar 24	N	N	0.58	0.61
MWC 137	06 18 45.5	+15 16 52	HAeBe(?)	1, 2	...	...	...	...	2010 Mar 19	N	N	0.54	0.51
IRAS 06210+1432	06 23 56.2	+14 30 28	HAeBe(?)	11, 12, 14	...	...	...	...	2010 Mar 19	N	N	0.56	0.53
IRAS 06245−1013	06 26 53.8	−10 15 34	HAeBe	11, 24	...	...	...	...	2010 Mar 23	N	N	0.44	0.58
Mon OB1 IRAS12 S1	06 30 49.0	+12 57 54	Class 0	9, 25	800	25	76	9	2010 May 9	N	N	0.65	0.63
VY Mon	06 31 06.9	+10 26 05	HAeBe(?)	1, 2	800	5	15849	5	2010 Mar 23	N	N	0.42	0.58
LkHα 215	06 32 41.8	+10 09 34	HAeBe	1, 2	800	5	2951	5	2010 Mar 21	N	N	0.51	0.63
MWC 147	06 33 05.2	+10 29 20	HAeBe	1, 2	800	2	10715	5	2010 Mar 23	N	N	0.44	0.62
R Mon	06 39 09.9	+08 44 11	HAeBe(?)	1, 2	800	5	2692	5	2010 Mar 24	N	N	0.38	0.46
V590 Mon	06 40 44.6	+09 48 02	HAeBe	1, 2	800	2	33	2	2010 Mar 23	N	N	0.42	0.59
IRAS 06382+1017	06 41 03.3	+10 15 01	Class I	17	580	15	110	17	2010 May 8	N	N	0.51	0.59
IRAS 06464−1644	06 48 41.8	−16 48 06	HAeBe	11	...	...	...	...	2010 May 16	N	N	0.42	0.61
IRAS 06475−0735	06 49 58.8	−07 38 52	HAeBe	11, 26	...	...	...	...	2010 May 24	N	N	0.64	0.69
IRAS 06491+0508	06 51 45.8	+05 05 04	HAeBe(?)	11, 12	...	...	...	...	2010 Mar 21	N	N	0.38	0.46
IRAS 06523−2458	06 54 26.8	−25 02 12	HAeBe	11, 12	...	...	...	...	2010 Mar 16	N	N	0.44	0.69
IRAS 06531−0305	06 55 39.3	−03 09 45	HAeBe	11	...	...	...	...	2010 Mar 24	N	N	0.66	0.69
IRAS 06562−0337	06 58 44.2	−03 41 09	HAeBe	11	...	...	...	...	2010 Mar 23	N	N	0.42	0.59
IRAS 06571−0441	06 59 34.8	+10 15 01	HAeBe	9, 27	1400	9	440	9	2010 May 8	Y	N	0.64	0.58
GU CMa	07 01 49.5	−11 18 03	HAeBe	1, 11	...	...	...	...	2010 Mar 21	N	N	0.42	0.55
LkHα 218	07 02 42.5	−11 26 12	HAeBe	1, 2, 11	1050	5	110	5	2010 Mar 24	N	N	0.58	0.63
Z CMa	07 03 43.2	−11 33 06	HAeBe	1	1050	5	427000	5	2010 Mar 21	N	N	0.45	0.56
LkHα 220	07 04 06.7	−11 26 09	HAeBe	1, 2, 11	1150	2	257	2	2010 Mar 18	N	N	0.38	0.56
MWC 166	07 04 25.5	−10 27 16	HAeBe	1, 11	...	...	...	...	2010 Mar 18	N	N	0.38	0.58
IRAS 07061−0414	07 08 38.8	−04 19 08	HAeBe	11	7950	15	...	...	2010 Mar 16	N	N	0.39	0.58
IRAS 07173−1733	07 19 35.9	−17 39 18	HAeBe(?)	11, 12, 14	...	...	...	...	2010 Mar 21	N	N	0.44	0.62
IRAS 07222−2610	07 24 16.9	−26 16 01	HAeBe	11	...	...	...	...	2010 Mar 23	N	N	0.47	0.69
IRAS 07225−2428	07 24 37.0	−24 34 48	HAeBe	11	...	...	...	...	2010 Mar 24	N	N	0.61	0.68
IRAS 07230−2539	07 25 04.9	−25 45 48	HAeBe	11, 26	...	...	...	...	2010 Mar 23	N	N	0.48	0.69
IRAS 07296−1921	07 31 48.9	−19 27 33	HAeBe	11	...	...	...	...	2010 Mar 23	N	N	0.45	0.64
IRAS 07303−2148	07 32 27.2	−21 55 27	HAeBe	11, 12	...	...	...	...	2010 Mar 21	N	N	0.48	0.64
IRAS 07394−1953	07 41 41.2	−20 00 14	HAeBe	11	...	...	...	...	2010 Mar 16	N	N	0.43	0.62
IRAS 15462−2551	15 49 15.3	−26 00 55	HAeBe	11, 26	...	...	...	...	2010 Mar 17	N	N	0.49	0.70
IRAS 15473−0346	15 49 57.7	−03 55 16	HAeBe	1, 11, 28	99	5	23	5	2010 Feb 22	N	N	0.65	1.02
IRAS 15537−2153	15 56 40.0	−22 01 40	HAeBe	1, 11, 12	145	5	17	5	2010 Mar 17	N	N	0.47	0.64
IRSA 16038−2735	16 06 58.0	−27 43 10	HAeBe	1, 11, 12	145	5	15	5	2010 Mar 17	N	N	0.51	0.76
IRAS 16102−2221	16 13 11.6	−22 29 07	HAeBe	11, 12	...	...	...	...	2010 Mar 19	N	N	0.44	0.59
IRAS 16156−2358	16 18 37.2	−24 05 18	HAeBe	11	...	...	...	...	2010 Mar 19	N	N	0.45	0.61
Elias 29	16 27 09.4	−24 37 19	Class I	8	160	8	41	8	2010 Jan 12	N	N	0.42	0.63
IRAS 16372−2347	16 40 17.9	−23 53 45	HAeBe	1, 11, 28	203	7	36	7	2010 Mar 19	N	N	0.47	0.62
KK Oph	17 10 08.1	−27 15 18	HAeBe(?)	1, 2	160	5	26	5	2010 Mar 17	N	N	0.39	0.64
IRAS 17178−2600	17 20 56.1	−26 03 31	HAeBe	11, 12	...	...	...	...	2010 Mar 17	N	N	0.39	0.61
IRAS 17423−1755	17 45 14.2	−17 56 47	HAeBe(?)	11, 12, 14	...	...	...	...	2010 Mar 17	N	N	0.43	0.64
IRAS 17481−1415	17 50 57.8	−14 16 11	HAeBe	11, 12	...	...	...	...	2010 Feb 22	N	N	0.42	0.59
MWC 275	17 56 21.3	−21 57 22	HAeBe	1, 11, 12	130	7	35	7	2010 Mar 18	N	N	0.36	0.53
IRAS 17575−1647	18 00 29.3	−16 47 23	HAeBe	11	...	...	...	...	2010 Mar 19	N	N	0.54	0.61
IRAS 18213−2948	18 24 29.8	−29 46 49	HAeBe	11, 12	145	5	18	5	2010 Mar 18	N	N	0.32	0.53
MWC 297	18 27 39.5	−03 49 52	HAeBe	1, 11, 28	280	23	220	23	2010 Feb 22	N	N	0.51	0.63

Table 1
(Continued)

Source	R.A.	Decl.	Source Type[a]	Ref.	Distance	Ref.	L_{bol}	Ref.	Observing	Detection		σ_{H_2O}	σ_{CH_3OH}
	(J2000)	(J2000)			(pc)		($L_\odot$)		Date	H_2O	CH_3OH	(Jy)	(Jy)
(1)	(2)	(3)	(4)	(5)	(6)	(7)	(8)	(9)	(10)	(11)	(12)	(13)	(14)
VV Ser	18 28 47.9	+00 08 40	HAeBe	1, 2, 11	614	7	336	7	2010 Feb 22	N	N	0.45	0.58
MWC 300	18 29 25.7	−06 04 37	HAeBe	1	...	...	...	...	2010 Mar 18	N	N	0.33	0.45
Serpens FIRS1	18 29 49.6	+01 15 22	Class 0	8	310	8	46	8	2010 May 8	Y	N	0.64	0.47
IRAS 18275+0040	18 30 06.2	+00 42 34	HAeBe	11	700	23	3.4	23	2010 Mar 18	N	N	0.32	0.44
AS 310	18 33 21.2	−04 58 02	HAeBe	1, 2	2500	5	162000	5	2010 Mar 17	N	N	0.43	0.55
IRAS 18391+0805	18 41 34.8	+08 08 22	HAeBe	11	...	...	...	...	2010 Mar 19	N	N	0.49	0.51
IRAS 18454+0250	18 48 00.4	+02 54 13	HAeBe	11	...	...	...	...	2010 Mar 19	N	N	0.53	0.51
IRAS 18483+0838	18 50 47.2	+08 42 10	HAeBe	11	...	...	...	...	2010 Mar 19	N	N	0.51	0.52
IRAS 18528+0400	18 55 23.0	+04 04 34	HAeBe	11	...	...	...	...	2010 Mar 17	N	N	0.39	0.53
MWC 614	19 11 11.3	+15 47 16	HAeBe	1, 11, 12	201	7	63	7	2010 Feb 24	N	N	0.43	0.55
WW Vul	19 25 58.8	+21 12 31	HAeBe	1, 2	696	7	50	7	2010 Feb 24	N	N	0.44	0.52
Par 21	19 29 00.7	+09 38 39	HAeBe	1	...	...	...	...	2010 Mar 19	N	N	0.33	0.41
IRAS 19343+2926	19 36 18.9	+29 32 50	HAeBe(?)	11, 12, 14	...	...	...	...	2010 Mar 18	N	N	0.31	0.40
HH 165	19 42 55.7	+23 24 20	HAeBe	8, 29	900	8	52	8	2010 May 7	Y[b]	N	0.38	0.41
V1295 Aql	20 03 02.5	+05 44 17	HAeBe	1, 11, 28	767	7	471	7	2010 Mar 17	N	N	0.38	0.49
IRAS 20050+2720 MMS1	20 07 06.7	+27 28 53	Class 0	8, 9, 30	700	8	305	8	2010 May 8	Y	N	0.58	0.52
V1685 Cyg	20 20 28.2	+41 21 52	HAeBe	1, 2	980	5	60300	5	2010 Apr 18	N	N	0.34	0.40
V1686 Cyg	20 20 29.3	+41 21 29	HAeBe	1, 28	980	5	257	5	2010 Apr 18	N	N	0.38	0.38
V1318 CygS	20 20 30.5	+41 21 27	HAeBe	31	1000	31	1600	31	2010 Apr 18	Y	Y[b]	0.59	0.56
BD+41°3731	20 24 15.7	+42 18 01	HAeBe	13	...	...	...	...	2010 Apr 17	N	N	0.53	0.52
Par 22	20 24 29.5	+42 14 02	HAeBe	1	...	...	...	...	2010 Mar 19	N	N	0.51	0.49
S106 FIR	20 27 25.4	+37 22 48	Class 0	8	600	8	<1080	8	2010 Jan 13	Y	N	0.38	0.47
PV Cep	20 45 54.0	+67 57 39	HAeBe(?)	1, 2	500	32	80	32	2010 Feb 22	N	N	0.43	0.52
V517 Cyg	20 47 23.3	+43 44 40	HAeBe	13	...	...	...	...	2010 Apr 17	N	N	0.51	0.53
AS 442	20 47 37.5	+43 47 25	HAeBe	1, 28	826	7	207	7	2010 Feb 24	N	N	0.44	0.51
LkHα 134	20 48 04.8	+43 47 26	HAeBe	1	700	5	5248	5	2010 Mar 19	N	N	0.38	0.44
LkHα 147	20 51 02.7	+43 49 32	HAeBe	1, 2	800	2	17378	2	2010 Mar 19	N	N	0.47	0.46
V1493 Cyg	20 52 04.6	+44 37 31	HAeBe(?)	1, 2	...	...	...	...	2010 Mar 19	N	N	0.58	0.56
V1057 Cyg	20 58 53.7	+44 15 29	HAeBe	13	700	32	540	32	2010 Apr 9	N	N	0.56	0.62
MWC 361	21 01 36.9	+68 09 48	HAeBe	1, 2	419	5	13804	5	2010 Mar 17	N	N	0.43	0.52
LkHα 324	21 03 54.2	+50 15 10	HAeBe	1, 2	780	5	912	5	2010 Feb 22	N	N	0.39	0.53
HD 203024	21 16 03.0	+68 54 52	HAeBe(?)	1, 28	...	...	...	...	2010 Mar 17	N	N	0.38	0.47
V645 Cyg	21 39 58.2	+50 14 21	HAeBe	1	3500	5	11749	5	2010 Feb 22	Y	N	0.45	0.53
IRAS 21391+5802	21 40 42.4	+58 16 10	Class 0	6, 8, 17	750	6	150	6	2010 May 7	Y	Y	0.47	0.53
V361 Cep	21 42 50.2	+66 06 35	HAeBe	1, 2	1250	5	9120	5	2010 May 8	N	N	0.72	0.70
NGC 7129 FIRS2	21 43 01.6	+66 03 26	Class 0	6, 8, 9	1250	6	500	6	2010 May 8	Y	Y	0.39	0.41
V373 Cep	21 43 06.7	+66 06 55	HAeBe	1, 2	1250	5	4677	5	2010 May 8	Y	N	0.77	0.81
AS 477	21 52 34.1	+47 13 44	HAeBe	1, 2	1200	5	1072	5	2010 Mar 19	N	N	0.61	0.55
LkHα 257	21 54 18.8	+47 12 10	HAeBe	1	...	...	...	...	2010 Mar 19	N	N	0.59	0.59
BH Cep	22 01 42.9	+69 44 37	HAeBe	1, 2	450	5	9	5	2010 Mar 17	N	N	0.27	0.34
IRAS 22176+6303	22 19 18.1	+63 18 49	Class I	8	910	8	337	8	2010 May 8	N	Y	0.59	0.61
SV Cep	22 21 33.2	+73 40 27	HAeBe	1, 2	596	7	38	7	2010 Mar 21	N	N	0.36	0.52
IRAS 22267+6244	22 28 29.3	+62 59 44	Class I	8, 33	900	33	310	33	2010 May 8	N	N	0.55	0.55
IRAS 22272+6358	22 28 52.2	+64 13 43	Class I	8, 33	950	33	815	33	2010 May 8	N	N	0.48	0.52
LkHα 233	22 34 41.0	+40 40 05	HAeBe	1, 2	880	5	93	5	2010 Mar 19	N	N	0.58	0.55
IRAS 22451+6154	22 47 02.1	+62 10 11	Class I	9, 17	1290	23	823	23	2010 May 8	N	N	0.49	0.51
IL Cep	22 53 15.6	+62 08 45	HAeBe	1	...	...	...	...	2010 Mar 17	N	N	0.43	0.52
IRAS 23011+6126	23 03 13.9	+61 42 21	Class 0	6, 8, 9	730	6	100	6	2010 Jan 14	N	Y[b]	0.26	0.33
BHJ 71	23 05 07.5	+62 15 37	HAeBe	1	...	...	...	...	2010 Mar 18	N	N	0.36	0.49
IRAS 23037+6213	23 05 50.3	+62 30 12	Class I	8, 33	750	8	129	8	2010 May 8	Y	N	0.49	0.49
MWC 1080	23 17 25.6	+60 50 44	HAeBe(?)	1, 2	2200	5	3388441	5	2010 Mar 18	N	N	0.36	0.51
LkHα 259	23 58 41.6	+66 26 13	HAeBe	1	...	...	...	...	2010 Mar 17	N	N	0.43	0.51

Notes.
[a] Sources with a question mark were classified as HAeBe candidates initially, but later analysis suggests they are not in the HAeBe stage.
[b] Newly detected objects in our survey.
[c] H_2O maser emission lines toward the position of NGC1333 IRAS2 were detected, but turned out to be the sidelobe effect by HH7-11C.
[d] H_2O maser emission lines toward the position of OMC3 MMS6, OMC3 MMS9, OMC3 MMS7, OMC2 FIR4, and T Ori were detected, but turned out to be the sidelobe effect by Orion KL.

References. (1) Thé et al. 1994; (2) Hernández et al. 2004; (3) Mannings & Sargent 2000; (4) Hernández et al. 2004; (5) Manoj et al. 2006; (6) Alonso-Albi et al. 2010; (7) Montesinos et al. 2009; (8) Furuya et al. 2003; (9) Froebrich 2005; (10) Chen et al. 2009; (11) Vieira et al. 2003; (12) Sartori et al. 2010; (13) Palla & Prusti 1993; (14) Vieira et al. 2011; (15) Yang et al. 2002; (16) Malfait et al. 1998; (17) Saraceno et al. 1996; (18) Beltrán et al. 2001; (19) Dent et al. 1998; (20) Chini et al. 2001; (21) Wu et al. 1996; (22) Sandell et al. 1999; (23) Connelley et al. 2008; (24) Gregorio-Hetem et al. 1992; (25) Wolf-Chase et al. 2003; (26) Torres et al. 1995; (27) Han et al. 1998; (28) Mora et al. 2001; (29) Dent & Aspin 1992; (30) Furuya et al. 2005; (31) Palla et al. 1995; (32) Wu et al. 2004; (33) Connelley et al. 2007.

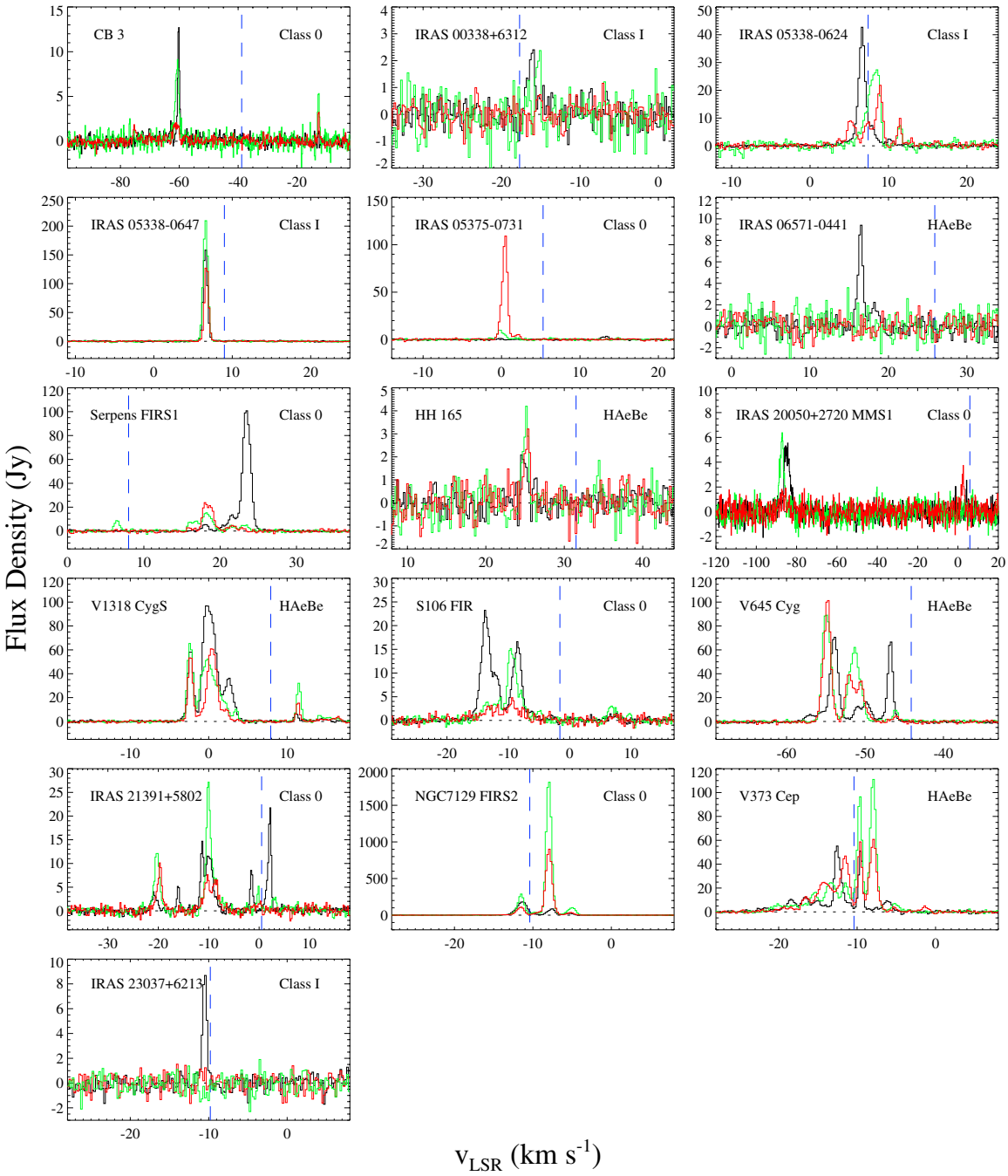

Figure 1. Spectra of the H_2O maser sources. In each panel, black, green, and red lines represent data obtained in the first, second, and third observation periods, respectively. Blue vertical dashed line indicates the systemic velocity of the parental dense molecular core. The evolutionary stage of the central object is shown at the upper right corner.

Table 2
Description of the Observations

Maser	Frequency (GHz)	FWHM ($''$)	η_a	Velocity Resolution (km s^{-1})	Velocity Coverage (km s^{-1})	System Temperature (K)
H_2O $6_{16}-5_{23}$	22.23508	130	0.72	0.105	432	60–150
CH_3OH $7_0-6_1A^+$	44.06943	65	0.69	0.053	218	120–210

Columns 3–5, the integrated line flux, peak intensity, and peak velocity in Columns 6–8, and the equivalent width ($\int F_\nu dv/F_{\rm peak}$) in Column 9.

Table 5 exhibits the detection rates of H_2O and CH_3OH masers for the sources in different evolutionary stages. The detection rates of both masers decrease substantially as the central (proto)stars evolve. The detection rate of H_2O masers is 50% for Class 0 objects, while the rates are 21% and 3% for Class I objects and HAeBe stars, respectively. This trend is also seen in the case of CH_3OH masers. The detection rate of

Table 3
H_2O Maser Line Parameters of Detected Sources

Source	Observing	Gaussian Fits			Integrated Lines			
	Date	$\int F_\nu dv$ (Jy km s^{-1})	$v_{\rm LSR}$ (km s^{-1})	δv (km s^{-1})	$\int F_\nu dv$ (Jy km s^{-1})	$F_{\rm peak}$ (Jy)	$v_{\rm peak}$ (km s^{-1})	Equivalent Width (km s^{-1})
(1)	(2)	(3)	(4)	(5)	(6)	(7)	(8)	(9)
CB 3	2010 May 7	10.54 ± 0.33	−60.24 ± 0.01	0.76 ± 0.03	11.21	12.65	−60.15	0.88
	2010 Oct 20	13.20 ± 0.55	−60.74 ± 0.03	1.43 ± 0.09	12.09	9.10	−60.57	1.32
		4.10 ± 0.44	−12.65 ± 0.04	0.66 ± 0.08	4.21	5.32	−12.53	0.78
	2010 Dec 2	1.88 ± 0.33	−75.13 ± 0.09	1.17 ± 0.23	1.77	1.77	−75.31	0.99
		4.55 ± 0.44	−61.16 ± 0.09	2.12 ± 0.20	4.21	2.10	−60.99	2.04
		1.77 ± 0.11	−12.62 ± 0.02	0.43 ± 0.05	1.88	3.33	−12.53	0.58
IRAS 00338+6312	2010 May 7	2.77 ± 0.33	−16.19 ± 0.07	1.16 ± 0.17	2.99	2.44	−15.91	1.23
	2010 Oct 20	1.55 ± 0.33	−15.39 ± 0.09	0.60 ± 0.21	1.66	2.44	−15.07	0.68
	2010 Dec 2	...	...	...	...	...	...	...
IRAS 05338−0624	2010 Jan 13	45.73 ± 0.44	6.64 ± 0.01	1.09 ± 0.01	54.05	42.62	6.64	1.26
	2010 Oct 20	48.50 ± 1.33	8.14 ± 0.02	1.69 ± 0.05	52.72	27.30	8.53	1.93
		4.10 ± 0.77	11.46 ± 0.05	0.54 ± 0.09	4.88	7.32	11.48	0.68
	2010 Dec 2	11.76 ± 0.55	5.27 ± 0.03	1.22 ± 0.08	12.09	8.99	5.16	1.35
		10.76 ± 0.88	7.42 ± 0.05	1.24 ± 0.12	8.54	8.54	7.48	1.00
		19.09 ± 0.66	8.89 ± 0.02	0.86 ± 0.04	21.09	21.86	8.95	0.97
		5.32 ± 0.44	11.42 ± 0.02	0.53 ± 0.05	5.32	9.87	11.48	0.55
IRAS 05338−0647	2010 May 8	104.34 ± 0.44	6.58 ± 0.01	0.64 ± 0.01	111.00	158.28	6.64	0.70
	2010 Oct 20	155.84 ± 0.44	6.60 ± 0.01	0.69 ± 0.01	155.51	209.45	6.64	0.74
	2010 Dec 2	86.24 ± 0.33	6.73 ± 0.01	0.60 ± 0.01	87.24	126.98	6.64	0.69
IRAS 05375−0731	2010 Jan 18	4.55 ± 0.33	13.25 ± 0.04	1.12 ± 0.10	4.55	3.44	13.38	1.32
	2010 Oct 20	10.76 ± 0.44	−0.09 ± 0.02	1.08 ± 0.06	11.32	9.87	−0.32	1.15
	2010 Dec 2	89.35 ± 0.44	0.04 ± 0.01	0.78 ± 0.01	92.01	109.22	0.53	0.84
		4.32 ± 0.44	2.04 ± 0.04	0.75 ± 0.07	4.88	5.32	2.21	0.92
IRAS 06571−0441	2010 May 7	7.77 ± 0.44	16.44 ± 0.02	0.75 ± 0.05	7.65	9.43	16.53	0.80
	2010 Oct 20	...	...	...	...	...	...	...
	2010 Dec 2	...	...	...	...	...	...	...
Serpens FIRS1	2010 May 8	5.66 ± 0.44	18.04 ± 0.03	0.96 ± 0.08	5.99	5.32	18.01	1.11
		26.41 ± 1.77	21.73 ± 0.07	2.10 ± 0.16	16.98	13.65	21.59	1.25
		132.86 ± 0.44	23.47 ± 0.01	1.22 ± 0.01	133.53	100.78	23.49	1.33
	2010 Oct 20	7.77 ± 0.55	6.48 ± 0.03	0.83 ± 0.06	7.88	8.43	6.43	0.90
		11.32 ± 0.88	16.43 ± 0.05	1.32 ± 0.11	12.43	8.32	16.96	1.48
		23.75 ± 0.99	18.31 ± 0.03	1.50 ± 0.07	22.53	15.42	18.22	1.47
		4.77 ± 0.77	21.51 ± 0.07	1.05 ± 0.17	5.10	4.77	21.38	1.05
		6.32 ± 0.77	23.20 ± 0.06	1.18 ± 0.16	5.99	5.10	23.49	1.18
	2010 Dec 2	2.10 ± 0.55	15.96 ± 0.11	0.64 ± 0.24	2.88	2.88	15.69	1.01
		38.62 ± 0.77	18.39 ± 0.02	1.51 ± 0.03	36.96	23.86	18.01	1.56
		6.32 ± 0.77	21.56 ± 0.07	1.27 ± 0.18	5.66	4.77	21.59	1.18
		1.66 ± 0.44	23.00 ± 0.09	0.59 ± 0.15	1.88	2.99	22.86	0.66
HH 165	2010 May 8	1.88 ± 0.33	24.86 ± 0.06	0.80 ± 0.11	1.66	2.10	24.54	0.82
	2010 Oct 20	3.33 ± 0.44	25.08 ± 0.05	0.83 ± 0.11	3.10	4.21	25.18	0.76
	2010 Dec 2	2.55 ± 0.44	25.27 ± 0.06	0.80 ± 0.14	2.55	3.33	25.39	0.79
IRAS 20050+2720 MMS1	2010 May 8	19.09 ± 0.77	−84.75 ± 0.07	3.59 ± 0.18	17.31	5.43	−84.37	3.13
	2010 Oct 20	15.54 ± 0.77	−87.33 ± 0.06	2.56 ± 0.15	14.98	6.43	−87.11	2.37
	2010 Dec 2	4.77 ± 0.55	2.40 ± 0.09	1.57 ± 0.21	4.32	3.77	2.63	1.17
V1318 CygS	2010 Apr 18	54.61 ± 0.44	−2.31 ± 0.01	0.85 ± 0.01	56.16	57.38	−2.21	0.97
		200.35 ± 0.77	0.08 ± 0.01	1.87 ± 0.01	191.47	96.23	−0.32	1.98
		61.93 ± 0.88	2.43 ± 0.01	1.70 ± 0.03	48.50	35.74	2.63	1.34
		4.21 ± 0.44	11.15 ± 0.03	0.58 ± 0.06	3.88	5.99	11.06	0.65
	2010 Oct 20	47.28 ± 0.55	−2.40 ± 0.01	0.71 ± 0.01	58.49	65.26	−2.42	0.89
		137.97 ± 0.99	0.04 ± 0.01	2.75 ± 0.03	130.75	52.39	−0.11	2.50
		6.32 ± 0.44	3.48 ± 0.02	0.63 ± 0.05	7.77	10.21	3.48	0.75
		20.53 ± 0.44	11.50 ± 0.01	0.60 ± 0.01	21.53	32.07	11.48	0.67
		7.65 ± 0.77	14.88 ± 0.13	2.30 ± 0.25	9.54	4.88	14.01	1.92
	2010 Dec 2	43.73 ± 0.44	−2.33 ± 0.01	0.73 ± 0.01	44.06	53.28	−2.42	0.83
		92.68 ± 0.77	0.43 ± 0.01	1.41 ± 0.01	97.79	60.82	0.32	1.60
		7.54 ± 0.44	2.25 ± 0.02	0.74 ± 0.05	6.66	10.21	2.21	0.66
		8.99 ± 0.44	11.38 ± 0.01	0.51 ± 0.03	9.54	15.42	11.48	0.62
		3.55 ± 0.77	16.26 ± 0.13	1.13 ± 0.28	4.10	4.32	16.54	0.93
S106 FIR	2010 Jan 13	41.62 ± 0.44	−13.68 ± 0.01	1.78 ± 0.03	39.84	23.31	−13.80	1.71
		22.75 ± 0.99	−12.32 ± 0.05	2.05 ± 0.11	12.43	10.10	−12.32	1.22
		30.30 ± 0.44	−8.58 ± 0.01	1.85 ± 0.03	29.85	16.53	−8.53	1.80
	2010 Oct 20	7.77 ± 1.22	−13.42 ± 0.18	2.08 ± 0.40	5.10	3.88	−13.38	1.30
		3.33 ± 0.99	−11.69 ± 0.15	0.98 ± 0.21	6.54	4.88	−11.27	1.34

Table 3
(Continued)

Source	Observing	Gaussian Fits			Integrated Lines			
	Date	$\int F_\nu dv$ (Jy km s^{-1})	$v_{\rm LSR}$ (km s^{-1})	δv (km s^{-1})	$\int F_\nu dv$ (Jy km s^{-1})	$F_{\rm peak}$ (Jy)	$v_{\rm peak}$ (km s^{-1})	Equivalent Width (km s^{-1})
(1)	(2)	(3)	(4)	(5)	(6)	(7)	(8)	(9)
		33.41 ± 1.44	−9.35 ± 0.04	2.40 ± 0.16	25.41	15.20	−9.59	1.67
		10.87 ± 3.10	−8.13 ± 0.26	1.90 ± 0.56	6.43	6.43	−7.90	1.01
		4.21 ± 0.55	6.89 ± 0.10	1.43 ± 0.22	4.10	2.99	6.85	1.34
	2010 Dec 2	4.77 ± 0.99	−13.18 ± 0.16	2.00 ± 0.54	4.10	3.10	−12.75	1.24
		0.88 ± 0.33	−11.77 ± 0.03	0.27 ± 0.10	2.22	3.33	−11.69	0.69
		8.88 ± 0.88	−9.32 ± 0.13	2.71 ± 0.38	7.65	4.77	−9.37	1.58
V645 Cyg	2010 Feb 22	11.21 ± 0.77	−56.92 ± 0.05	1.70 ± 0.13	7.54	5.99	−56.99	1.24
		90.68 ± 0.55	−53.92 ± 0.01	1.20 ± 0.01	97.79	70.48	−53.83	1.39
		18.64 ± 0.77	−50.85 ± 0.02	1.32 ± 0.06	12.65	12.65	−50.88	1.00
		24.19 ± 0.55	−49.83 ± 0.02	1.38 ± 0.05	19.42	16.42	−49.82	1.18
		56.16 ± 0.33	−46.76 ± 0.01	0.78 ± 0.01	58.60	66.60	−46.66	0.88
	2010 Oct 20	120.99 ± 0.77	−54.90 ± 0.01	1.23 ± 0.01	122.76	89.02	−54.88	1.38
		103.23 ± 0.88	−51.32 ± 0.01	1.65 ± 0.02	104.34	62.04	−51.30	1.68
		6.66 ± 0.55	−46.09 ± 0.01	0.65 ± 0.07	7.54	9.43	−46.24	0.80
	2010 Dec 2	115.66 ± 0.55	−54.81 ± 0.01	1.09 ± 0.01	117.66	101.12	−54.67	1.16
		44.51 ± 0.99	−52.03 ± 0.02	1.07 ± 0.03	51.72	39.18	−51.93	1.32
		44.62 ± 1.22	−50.58 ± 0.02	1.32 ± 0.05	38.07	33.85	−50.46	1.12
		4.32 ± 0.55	−46.03 ± 0.07	0.93 ± 0.19	4.32	4.77	−46.03	0.91
IRAS 21391+5802	2010 May 7	5.10 ± 0.44	−20.79 ± 0.05	1.37 ± 0.13	4.77	4.10	−20.96	1.17
		3.33 ± 0.33	−16.04 ± 0.02	0.54 ± 0.05	3.44	5.21	−15.91	0.66
		13.87 ± 0.44	−11.23 ± 0.01	0.96 ± 0.03	10.87	14.65	−11.27	0.74
		23.19 ± 0.77	−9.96 ± 0.03	1.88 ± 0.07	20.42	11.43	−10.22	1.77
		5.66 ± 0.33	−1.51 ± 0.01	0.61 ± 0.04	5.88	8.43	−1.58	0.68
		15.65 ± 0.33	2.11 ± 0.01	0.71 ± 0.02	17.31	21.86	2.21	0.80
	2010 Oct 20	15.98 ± 0.55	−20.26 ± 0.02	1.25 ± 0.06	16.76	12.09	−20.12	1.38
		33.85 ± 0.55	−9.99 ± 0.01	1.32 ± 0.04	41.07	27.08	−10.01	1.51
		2.66 ± 0.44	−0.17 ± 0.04	0.57 ± 0.14	3.33	5.21	−0.11	0.63
		2.55 ± 0.44	3.01 ± 0.08	0.87 ± 0.16	2.66	2.88	3.27	0.91
	2010 Dec 2	9.10 ± 0.55	−19.71 ± 0.03	0.99 ± 0.09	11.98	10.10	−19.70	1.17
		8.32 ± 0.88	−10.32 ± 0.06	1.25 ± 0.17	10.54	7.65	−10.22	1.36
		7.54 ± 0.88	−8.66 ± 0.07	1.19 ± 0.16	8.32	6.54	−8.74	1.28
NGC 7129 FIRS2	2010 May 8	295.26 ± 0.88	−11.40 ± 0.01	1.54 ± 0.01	310.35	188.47	−11.27	1.65
		101.12 ± 0.55	−7.65 ± 0.01	1.13 ± 0.01	55.94	87.13	−7.48	0.64
		37.85 ± 0.77	−5.48 ± 0.01	1.41 ± 0.03	37.74	24.42	−5.37	1.54
	2010 Oct 20	286.71 ± 2.22	−11.52 ± 0.01	0.97 ± 0.01	297.25	288.93	−11.48	1.03
		1618.49 ± 1.99	−7.97 ± 0.01	0.81 ± 0.01	1632.03	1814.96	−7.90	0.90
		130.64 ± 2.55	−5.06 ± 0.01	1.22 ± 0.03	132.09	103.11	−4.95	1.28
	2010 Dec 2	126.31 ± 2.77	−11.61 ± 0.01	1.12 ± 0.03	134.19	110.00	−11.48	1.22
		908.09 ± 2.55	−7.96 ± 0.01	0.95 ± 0.01	955.26	900.98	−7.90	1.06
		34.63 ± 2.77	−5.22 ± 0.04	0.96 ± 0.10	40.73	37.07	−5.16	1.10
V373 Cep	2010 May 8	5.99 ± 1.22	−21.84 ± 0.18	1.80 ± 0.52	4.66	3.44	−21.80	1.33
		18.31 ± 1.44	−18.38 ± 0.06	1.82 ± 0.18	14.43	10.65	−18.43	1.37
		18.42 ± 1.22	−16.60 ± 0.04	1.44 ± 0.12	14.98	12.54	−16.54	1.20
		25.75 ± 3.33	−15.30 ± 0.14	2.98 ± 0.49	12.54	9.32	−15.06	1.34
		59.94 ± 0.88	−12.47 ± 0.01	1.07 ± 0.02	66.04	55.27	−12.53	1.20
		33.41 ± 0.44	−9.55 ± 0.01	0.61 ± 0.01	34.52	50.83	−9.59	0.68
		13.87 ± 0.88	−6.21 ± 0.05	1.52 ± 0.13	14.87	9.43	−6.21	1.56
	2010 Oct 20	22.42 ± 0.99	−15.50 ± 0.03	1.42 ± 0.08	22.08	16.42	−15.27	1.34
		40.95 ± 1.44	−13.34 ± 0.02	1.54 ± 0.07	39.96	24.42	−13.38	1.63
		28.52 ± 1.11	−11.42 ± 0.02	1.26 ± 0.06	27.97	24.30	−11.48	1.15
		78.14 ± 0.11	−9.67 ± 0.01	0.78 ± 0.01	79.80	96.34	−9.59	0.83
		104.67 ± 0.77	−7.96 ± 0.01	0.88 ± 0.01	109.00	118.21	−7.90	0.92
		7.54 ± 0.88	−5.15 ± 0.02	1.12 ± 0.17	8.99	6.99	−5.16	1.27
	2010 Dec 2	11.10 ± 0.99	−16.64 ± 0.04	0.99 ± 0.09	14.20	14.31	−16.54	0.99
		66.60 ± 2.10	−14.01 ± 0.04	2.62 ± 0.11	54.05	24.75	−14.22	2.18
		57.27 ± 1.55	−11.52 ± 0.01	1.24 ± 0.03	69.15	46.95	−11.48	1.48
		38.73 ± 0.55	−9.63 ± 0.01	0.64 ± 0.01	41.18	58.60	−9.59	0.70
		67.48 ± 0.88	−7.95 ± 0.01	1.07 ± 0.02	68.04	60.82	−7.90	1.13
		2.10 ± 0.55	−5.24 ± 0.08	0.55 ± 0.22	3.33	4.10	−5.37	0.80
		3.44 ± 0.77	−1.34 ± 0.08	0.81 ± 0.19	4.88	5.21	−1.37	0.97
IRAS 23037+6213	2010 May 8	6.10 ± 0.33	−10.50 ± 0.02	0.63 ± 0.04	6.43	8.65	−10.43	0.73
	2010 Oct 20	...	...	...	...	...	...	...
	2010 Dec 2	...	...	...	...	...	...	...

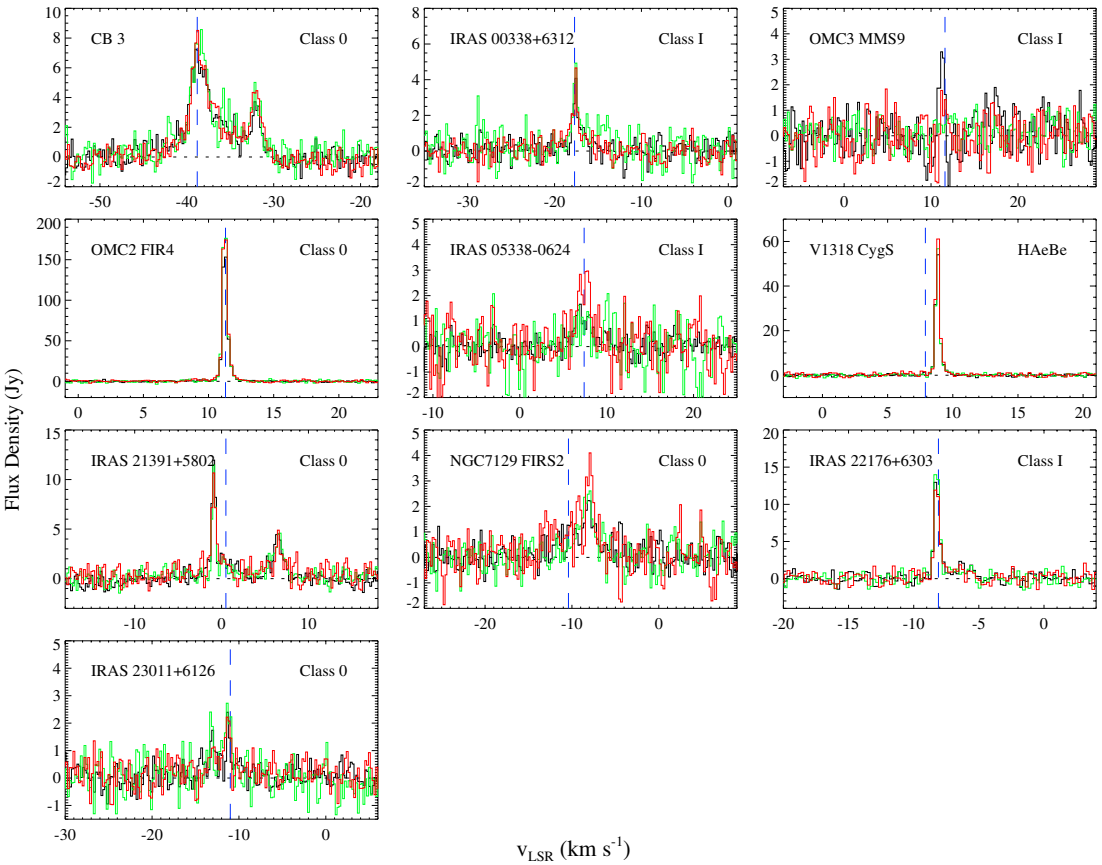

Figure 2. Same as in Figure 1 but for spectra of the 44 GHz Class I CH_3OH maser sources.

CH_3OH masers toward Class 0 objects is 36%, which is much higher than those of Class I (21%) and HAeBe (1%) sources.

It should be noted that the detection rates of H_2O and 44 GHz CH_3OH masers for HAeBe stars and candidates in our survey might be the lower limits for bona fide intermediate-mass PMS stars. Although the classification criteria introduced in Section 1 were intended to identify IMYSOs, some of the HAeBe candidates in our sample may not be in the PMS phase. The classification criteria allow contamination with objects such as post-asymptotic giant branch stars and protoplanetary nebulae, which could exhibit similar observational features (Thé et al. 1994; Sartori et al. 2010; Vieira et al. 2011). For example, Sartori et al. (2010) tested the young nature of 93 HAeBe candidates selected from the sample of Vieira et al. (2003), and concluded that at least 71 (76%) sources are PMS stars but 7 sources are evolved stars. Our sample contains 22 (15%) sources with ambiguity in their classification. They are indicated with question marks in Column 4 of Table 1. None of them show H_2O or CH_3OH maser emission. Even after accounting for this contamination, however, the detection rates of both masers toward intermediate PMS stars would still be much lower than those of Class 0 and Class I objects.

In this survey, we report the first detection of H_2O maser emission in one source (HH 165) and of 44 GHz CH_3OH maser emission in six sources (CB 3, IRAS 00338+6312, OMC3 MMS9, IRAS 05338−0624, V1318 CygS, and IRAS 23011+6126). We focus on two HAeBe stars, HH 165 and V1318 CygS, because *no* HAeBe star has previously been found to show 44 GHz CH_3OH maser emission and *only eight* HAeBe stars have been reported to show 22 GHz H_2O maser emission: LkHα 198, HD 250550, V373 Cep (Schwartz & Buhl 1975), IRAS 06571−0441 (Han et al. 1998), V1318 CygS (Palla et al. 1995), PV Cep (Torrelles et al. 1986), V1057 Cyg (Rodriguez et al. 1987), and V645 Cyg (Lada et al. 1981). Table 6 lists the eight with the detected line parameters. We observed all of them but did not detect any appreciable (>1 Jy) H_2O and CH_3OH maser emission from four of them: LkHα 198, HD 250550, PV Cep, and V1057 Cyg.

4.2. Notes on Some Individual Sources

As mentioned in the previous section, some sources are located within a single beam or the first sidelobe so that it is not straightforward to interpret the observational results. In order to determine genuine maser-emitting source(s) in such cases, we observed closely located objects successively and examined the detected maser lines of the individual sources. In the process, we assumed that the main beam of the telescope is Gaussian and used the FWHMs listed in Table 2, 130″ at 22 GHz and 65″ at 44 GHz.

4.2.1. IRAS 05338−0647 and HH147 MMS

IRAS 05338−0647 coincides with the ridge that contains HH 1−2 MMS 2−3 while HH147 MMS (≡ IRAS 05339−0646) corresponds to a YSO, which drives the HH147 bipolar outflow (Strom et al. 1985; Eislöfell et al. 1994; Chini et al. 2001). These two objects are 121″ apart from each other. Figure 3 displays the single H_2O maser lines detected toward these sources over three epochs. The two maser lines have practically the same velocity and line profile in each epoch. This strongly suggests that they are not distinct maser sources but rather are a single maser. However, it should be noted that the observed peak intensity ratio

Table 4
CH_3OH Maser Line Parameters of Detected Sources

Source	Observing	Gaussian Fits			Integrated Lines			
	Date	$\int F_v dv$ (Jy km s^{-1})	v_{LSR} (km s^{-1})	δv (km s^{-1})	$\int F_v dv$ (Jy km s^{-1})	F_{peak} (Jy)	v_{peak} (km s^{-1})	Equivalent Width (km s^{-1})
(1)	(2)	(3)	(4)	(5)	(6)	(7)	(8)	(9)
CB 3	2010 May 7	23.20 ± 0.92	-38.38 ± 0.07	3.82 ± 0.20	20.64	7.19	−38.96	2.87
		4.87 ± 0.46	-32.01 ± 0.06	1.28 ± 0.17	6.14	3.71	−32.15	1.62
	2010 Oct 20	18.09 ± 1.04	-38.52 ± 0.06	2.17 ± 0.15	18.21	8.58	−38.32	2.12
		6.61 ± 1.27	-35.23 ± 0.21	2.52 ± 0.72	4.06	4.75	−35.77	0.88
		6.26 ± 0.92	-32.08 ± 0.10	1.48 ± 0.31	5.56	4.98	−32.15	1.11
	2010 Dec 2	22.04 ± 0.81	-38.36 ± 0.06	3.27 ± 0.16	20.41	8.58	−38.74	2.39
		8.46 ± 0.81	-32.14 ± 0.08	2.05 ± 0.26	7.65	4.52	−31.94	1.72
IRAS 00338+6312	2010 May 7	3.48 ± 0.34	-17.58 ± 0.03	0.78 ± 0.10	3.24	4.06	−17.54	0.81
	2010 Oct 20	3.82 ± 0.58	-17.58 ± 0.06	0.88 ± 0.20	3.71	4.98	−17.54	0.77
	2010 Dec 2	4.06 ± 0.58	-17.65 ± 0.07	1.40 ± 0.33	4.29	4.75	−17.54	0.92
OMC3 MMS9	2010 May 6	2.32 ± 0.34	11.23 ± 0.06	0.64 ± 0.10	2.32	3.24	11.21	0.70
	2010 Oct 20	...	...	...	...	...	...	...
	2010 Dec 2	...	...	...	...	...	...	...
OMC2 FIR4	2010 May 6	81.78 ± 0.58	11.25 ± 0.01	0.45 ± 0.01	86.18	153.35	11.33	0.56
	2010 Oct 20	93.38 ± 0.58	11.25 ± 0.01	0.44 ± 0.01	97.78	176.32	11.33	0.55
	2010 Dec 2	92.80 ± 0.58	11.25 ± 0.01	0.44 ± 0.01	99.18	174.34	11.33	0.57
IRAS 05338−0624	2010 Jan 13	1.97 ± 0.34	6.87 ± 0.10	1.34 ± 0.34	1.74	1.74	6.96	1.07
		1.16 ± 0.34	7.95 ± 0.10	0.86 ± 0.30	1.04	1.27	8.03	0.82
	2010 Oct 20	...	...	...	...	...	...	...
	2010 Dec 2	1.85 ± 1.04	6.87 ± 0.15	0.71 ± 0.42	2.20	2.90	6.96	0.75
		2.55 ± 1.04	7.81 ± 0.13	0.79 ± 0.42	2.32	3.01	7.81	0.77
V1318 CygS	2010 Apr 18	22.27 ± 0.11	8.83 ± 0.01	0.37 ± 0.01	25.05	54.17	8.88	0.46
	2010 Oct 20	22.50 ± 0.34	8.83 ± 0.01	0.36 ± 0.01	24.70	56.72	8.88	0.43
	2010 Dec 2	24.47 ± 0.34	8.84 ± 0.01	0.37 ± 0.01	27.95	61.13	8.88	0.46
IRAS 21391+5802	2010 May 7	7.19 ± 0.46	-0.90 ± 0.02	0.56 ± 0.04	7.65	11.94	−0.90	0.64
		6.84 ± 0.58	6.48 ± 0.06	1.56 ± 0.16	6.61	4.52	6.54	1.44
	2010 Oct 20	5.56 ± 0.34	-0.88 ± 0.01	0.47 ± 0.03	5.68	11.36	−0.90	0.51
		6.38 ± 0.58	6.50 ± 0.07	1.63 ± 0.18	6.72	4.52	6.75	1.44
	2010 Dec 2	6.96 ± 0.34	-0.89 ± 0.03	0.67 ± 0.04	7.54	10.55	−0.90	0.70
		2.66 ± 0.58	6.50 ± 0.06	0.56 ± 0.17	3.24	4.87	6.54	0.68
NGC 7129 FIRS2	2010 May 8	3.24 ± 0.46	-8.04 ± 0.10	1.52 ± 0.26	3.01	2.20	−8.13	1.36
	2010 Oct 20	4.87 ± 0.58	-8.30 ± 0.12	2.09 ± 0.35	4.52	2.66	−7.92	1.75
	2010 Dec 2	3.59 ± 0.58	-7.93 ± 0.07	0.96 ± 0.15	3.48	4.06	−7.92	0.84
IRAS 22176+6303	2010 May 8	7.30 ± 0.34	-8.23 ± 0.01	0.50 ± 0.03	7.65	12.99	−8.34	0.59
	2010 Oct 20	8.00 ± 0.34	-8.23 ± 0.01	0.48 ± 0.02	8.00	14.15	−8.34	0.57
	2010 Dec 2	6.72 ± 0.46	-8.23 ± 0.02	0.49 ± 0.04	7.19	11.83	−8.34	0.61
IRAS 23011+6126	2010 Jan 14	1.27 ± 0.34	-13.01 ± 0.08	0.76 ± 0.27	1.16	1.74	−13.05	0.67
		1.16 ± 0.11	-11.28 ± 0.03	0.41 ± 0.09	1.16	2.32	−11.35	0.49
	2010 Oct 20	1.16 ± 0.23	-13.19 ± 0.05	0.37 ± 0.15	1.50	2.32	−13.27	0.56
		3.13 ± 0.46	-11.34 ± 0.10	1.20 ± 0.25	2.90	2.66	−11.35	1.10
	2010 Dec 2	1.97 ± 0.46	-11.34 ± 0.08	0.84 ± 0.25	1.85	2.20	−11.35	0.88

Table 5
Detection Rates of H_2O and CH_3OH Masers

Source Type	Number of Sources	H_2O (%)	CH_3OH (%)
Class 0	14	50 (7/14)	36 (5/14)
Class I	19	21 (4/19)	21 (4/19)
HAeBe	147	3 (5/147)	1 (1/147)
Total	180	9 (16/180)	6 (10/180)

of HH147 MMS to IRAS 05338−0647 changes considerably over the observations, 25% in 2010 May, 12% in October, and 17% in December. If the maser is variable but stays at the same position, the peak intensities of the two objects can vary but the ratio should be constant. These large intensity ratio variations can be explained only by $\gtrsim 10''$ pointing offsets even though off-center pointing is considered. It is also very *unlikely* that the large ratio variations were caused by the movement of a single maser, because the typical proper motion of a maser observed in other star-forming regions is only $\sim 0''.01\ \mathrm{yr}^{-1}$ (e.g., Hirota et al. 2007). Therefore, it is more plausible that the maser emission in the latter epoch was emitted from a new maser source formed after the disappearance of the maser source in the former epoch. Taking the intensity ratios into account, the masers seem to be located between the two objects, much closer to IRAS 05338−0647. This is consistent with the result of the grid mapping presented in Figure 4, which was made in the first epoch to investigate the existence of a nearby strong maser source (see Section 3).

4.2.2. V1685 Cyg, V1686 Cyg, and V1318 CygS

BD+40° is an active star-forming region, which contains at least 33 optical and NIR sources in a $\sim 1' \times 2'$ field, including 3 HAeBe stars: V1685 Cyg (≡ BD+40°4124), V1686 Cyg

Table 6
Previously Known Herbig Ae/Be Stars with H_2O Masers

Source	R.A. (J2000)	Decl. (J2000)	Observing Date	v_{LSR} (km s^{-1})	F_{peak} (Jy)	Ref.
LkHα 198	00 06 06[a]	+58 17 00[a]	1974 Sep 6	15	3	1
HD 250550	05 56 12[a]	+16 31 00[a]	1975 Apr 20	13	1.5	1
IRAS 06571−0441	06 57 06.4	−04 41 48	1993 Nov 23	−23.5	47.9	2
V1318 CygS	20 20 30.5	+41 21 27	1992 Nov 24	−80.5	13	3
	20 20 30.6	+41 21 26	2002 Sep 9	5.8[b]	46.7[b]	4
PV Cep	20 45 21.5	+67 46 41	1984 Jun 26	−3	160	5
				3	55	5
V1057 Cyg	20 57 06.2	+44 03 46	1984 Jan	... [c]	... [c]	6
V645 Cyg	21 38 10.6	+50 00 43	1979 Jan	−50.2	42	7
				−48.9	3	7
				−44.5	13	7
V373 Cep	21 40 48[a]	+65 39 00[a]	1975 Jun 8	−10.0	5	1

Notes.
[a] Coordinates are based on the B1900 equatorial system.
[b] We only provide the strongest component. See Marvel (2005) for the full list of maser components.
[c] Rodriguez et al. (1987) provided an H_2O maser position, but no maser line parameters.
References. (1) Schwartz & Buhl 1975; (2) Han et al. 1998; (3) Palla et al. 1995; (4) Marvel 2005; (5) Torrelles et al. 1986; (6) Rodriguez et al. 1987; (7) Lada et al. 1981.

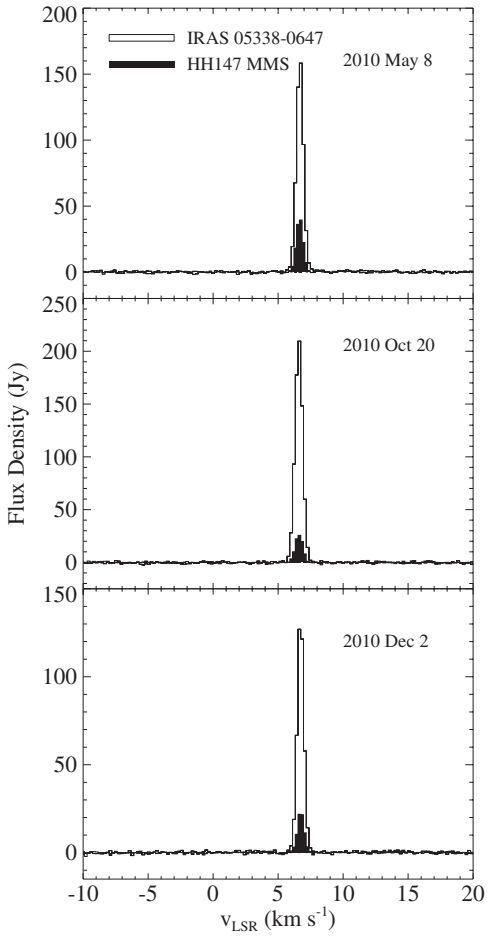

Figure 3. Spectra of the H_2O maser emission detected toward IRAS 05338−0647 and HH147 MMS.

(≡ LkHα 224), and V1318 CygS (≡ LkHα 225S) (Hillenbrand et al. 1995). Using the Medicina 32 m telescope, Palla & Prusti (1993) first detected H_2O maser emission toward BD+40° and claimed the maser emission stems from V1685 Cyg. However, Palla et al. (1995) observed this region in the H_2O maser line at ∼0.″1 spatial resolution using the Very Large Array (VLA), and found that the maser is coincident with V1318 CygS rather than V1685 Cyg. Marvel (2005) also detected H_2O maser emission toward V1318 CygS, in the v_{LSR} range between −80 km s^{-1} and +20 km s^{-1}, using the VLA and the Very Long Baseline Array.

We observed all three HAeBe stars on the same days and detected both H_2O and CH_3OH maser lines toward all of them (Figure 5). Assuming that the maser emission emanates from V1318 CygS, we estimated the expected line intensities at V1685 Cyg and V1686 Cyg, which are 36″ and 14″ from V1318 CygS on the sky, respectively. If the pointing accuracy is 5″, ∼81% ± 5% at 22 GHz and ∼43% ± 10% at 44 GHz of the original signal would be detected toward V1685 Cyg. In the case of V1686 Cyg, the values are ∼97% ± 2% lower at 22 GHz and ∼88% ± 8% at 44 GHz. Table 7 displays the observed and expected intensities. The observed intensities of the individual H_2O and CH_3OH maser lines are in very good agreement with the expected intensities for all three observations. This strongly suggests that all the CH_3OH maser lines detected toward these three HAeBe stars originate from V1318 CygS. Interferometric observations will be required to clarify this issue.

4.2.3. NGC 7129 FIRS2, V373 Cep, and V361 Cep

NGC 7129 is a reflection nebula illuminated by several stars including one Class 0 object, NGC 7129 FIRS2 (Eiora et al. 1998), and two HAeBe stars, V361 Cep and V373 Cep (≡ LkHα 234). Cesarsky et al. (1978) detected H_2O maser emission toward NGC 7129 FIRS2 and V373 Cep. However, we detected H_2O maser emission toward V361 Cep as well as the other two sources (Figure 6). The separation angles of V361 Cep from NGC 7129 FIRS2 and V373 Cep are 201″ and 102″, respectively. Since the KVN telescope has the first sidelobe with an attenuation of 14 dB at ∼1.5 times FWHM away from the main beam center, as noted earlier, ∼3.9% ± 0.2% of the H_2O maser emission from NGC 7129 FIRS2 and ∼18% ± 3% of the H_2O maser emission from V373 Cep would be detected toward V361 Cep. Table 8 presents both the observed maser line intensities of the three objects and the theoretically expected

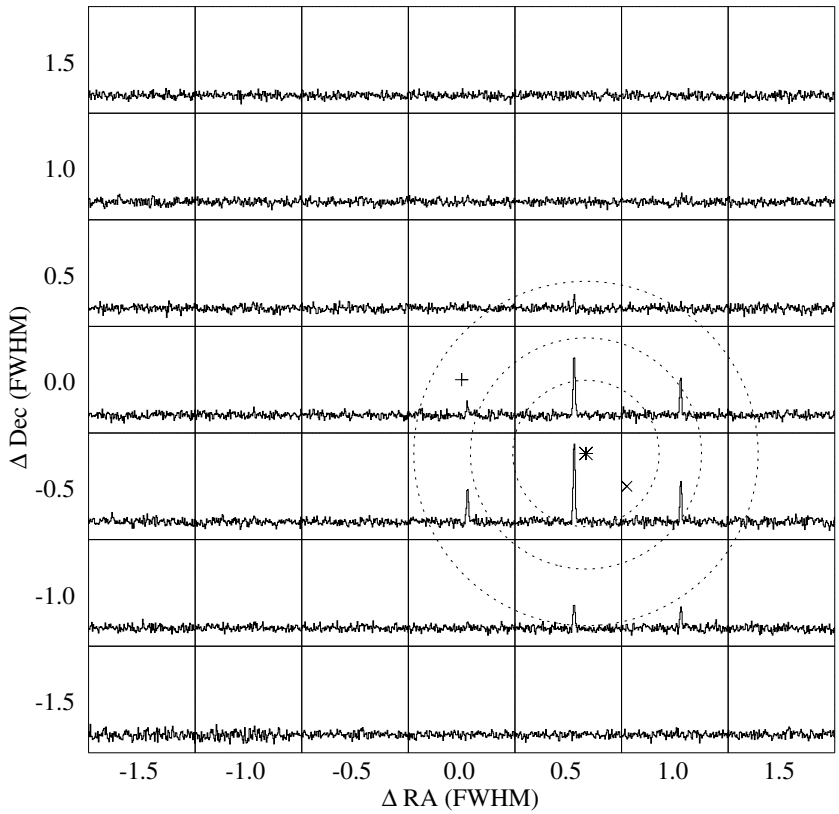

Figure 4. Grid mapping results of H_2O maser emission from HH147 MMS at the center (0.0, 0.0). The intensity pattern is well fitted by a two-dimensional Gaussian model with a similar FWHM to that presented in Table 2. The result is shown as dotted contours. Contour levels are 25%, 50%, and 75% of the Gaussian peak. The position of HH147 MMS is indicated with a plus symbol, while that of IRAS 05338−0647 is marked by a cross symbol. The asterisk symbol represents the position of the Gaussian peak. In each panel the horizontal and vertical axes are v_{LSR} and flux density, respectively. The v_{LSR} range is (−10 to +20) km s^{-1}, while the flux density range is (−30 to +220) Jy.

Table 7
Observed H_2O and CH_3OH Maser Line Intensities toward BD+40°

Observing	Line	Frequency	v_{LSR}	V1318 CygS	V1685 Cyg		V1686 Cyg	
Date	Number[a]	(GHz)	(km s^{-1})	F_{peak} (Jy)	F_{peak} (Jy)	Theoretical Estimation (Jy)	F_{peak} (Jy)	Theoretical Estimation (Jy)
2010 Apr 18	1	22.23508	−2.11	57.38	47.28	46.39 ± 2.74	55.38	55.65 ± 1.25
	2	22.23508	−0.21	96.23	75.70	77.80 ± 4.59	91.35	93.33 ± 2.09
	3	22.23508	+2.74	35.74	29.19	28.90 ± 1.71	35.18	34.66 ± 0.78
	4	22.23508	+11.17	5.99	4.77	4.84 ± 0.29	5.32	5.81 ± 0.13
	5	44.06943	+8.93	54.17	26.21	23.15 ± 5.47	49.99	47.93 ± 4.30
2010 Oct 20	1	22.23508	−2.42	65.26	55.05	52.76 ± 3.12	63.38	63.29 ± 1.42
	2	22.23508	−0.11	52.39	44.62	42.36 ± 2.50	49.50	50.81 ± 1.14
	3	22.23508	+3.48	10.21	8.54	8.26 ± 0.49	9.99	9.90 ± 0.22
	4	22.23508	+11.48	32.07	25.75	25.93 ± 1.53	29.97	31.10 ± 0.70
	5	22.23508	+14.01	4.88	4.21	3.95 ± 0.23	4.66	4.73 ± 0.11
	6	44.06943	+8.88	56.72	19.72	24.24 ± 5.73	45.47	50.18 ± 4.50
2010 Dec 2	1	22.23508	−2.42	53.28	44.51	43.08 ± 2.54	52.61	51.67 ± 1.16
	2	22.23508	+0.32	60.82	51.17	49.17 ± 2.90	59.16	59.08 ± 1.32
	3	22.23508	+2.21	10.21	7.88	8.26 ± 0.49	9.99	9.90 ± 0.22
	4	22.23508	+11.48	15.42	13.65	12.47 ± 0.74	14.76	14.96 ± 0.34
	5	22.23508	+16.54	4.32	3.44	3.49 ± 0.21	4.32	4.19 ± 0.09
	6	44.06943	+8.84	61.13	32.59	26.12 ± 6.17	56.72	54.09 ± 4.85

Note. [a] Numbers of each line are displayed in Figure 5.

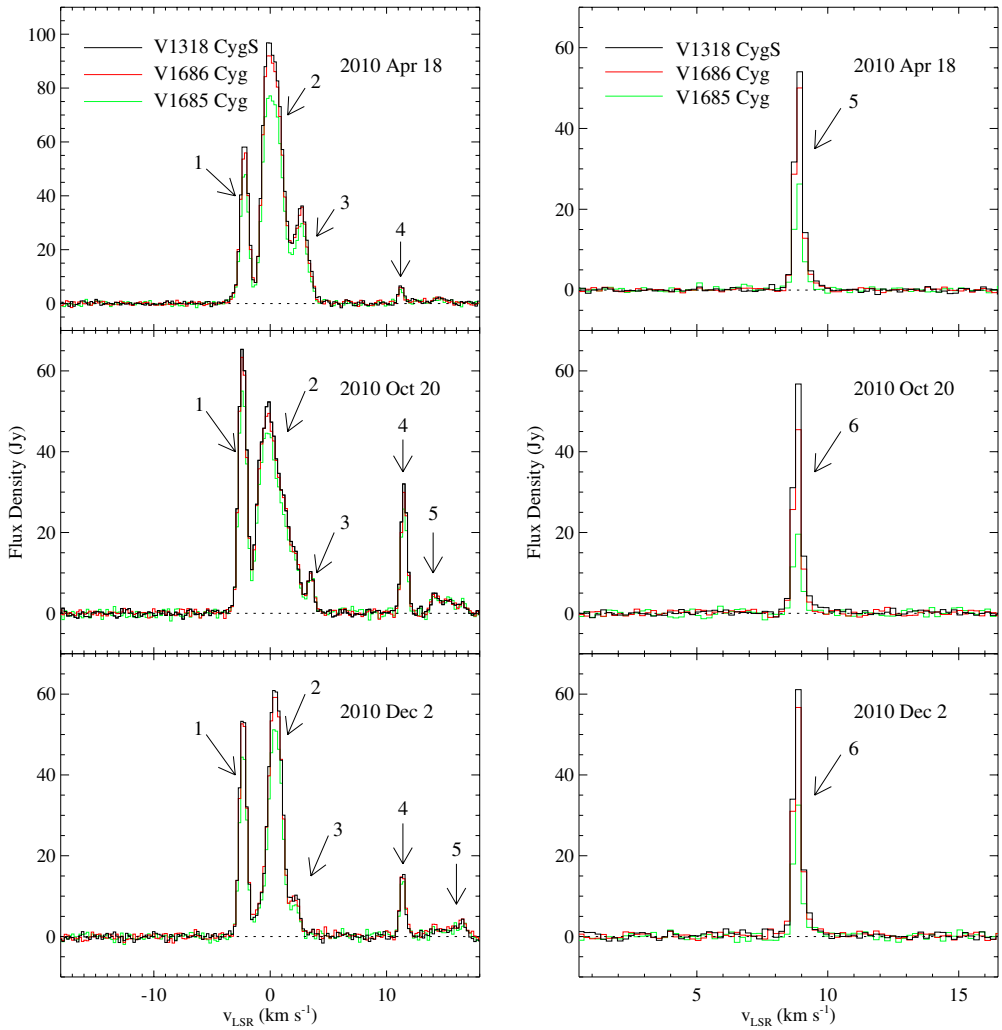

Figure 5. Left: spectra of the H_2O maser emission detected toward three HAeBe stars located in the BD+40° region, V1318 CygS (black lines), V1686 Cyg (red lines), and V1685 Cyg (green lines). Right: spectra of the CH_3OH maser emission.
(A color version of this figure is available in the online journal.)

values. They match well with each other. Therefore, it seems that the H_2O maser emission arises only from NGC 7129 FIRS2 and V373 Cep.

5. DISCUSSION

5.1. Detection Rates

As mentioned in Section 4.1, the overall detection rates of H_2O and CH_3OH masers in this study are 9% and 6%, respectively. If only Class 0 and Class I sources are included, the rates are 33% for H_2O and 27% for CH_3OH. For comparison, Wilking et al. (1994) made a multi-epoch H_2O maser line survey of 42 nearby ($d < 450$ pc) Class I sources with $L_{FIR} < 120\ L_\odot$, and detected maser emission in 36% of them. Furuya et al. (2001) also observed H_2O maser emission toward 30 Class 0 and 33 Class I objects with $L_{FIR} < 100\ L_\odot$. The detection rate was 21%. On the other hand, Sridharan et al. (2002) detected H_2O masers in 42% of 84 high-mass protostellar candidates. Szymczak et al. (2005) also detected 52% in a sample of 79 Class II CH_3OH maser sources at 6.7 GHz, which may trace an earlier stage of high-mass star formation than UCHII regions. Both surveys were made with the Effelsberg 100 m telescope. In the case of UCHII regions, whose ionizing stars have already reached the main sequence, the detection rate appears to be much higher. Churchwell et al. (1990) detected H_2O maser emission in 67% of 84 UCHII regions with a similar flux limit (mean rms $\sim$ 0.2 Jy at a velocity resolution of $\sim$0.2 km s^{-1}) to those of Sridharan et al. (2002) and Szymczak et al. (2005), using the same telescope. This is contrary to the results of the low- and intermediate-mass regime where the detection rates rapidly decrease after the central stars reach the PMS stage. We detected H_2O maser emission in only 3% of 147 HAeBe stars (intermediate-mass PMS stars) and Furuya et al. (2001) detected none in a sample of 9 Class II sources (low-mass PMS stars).

A similar trend is seen in 44 GHz Class I CH_3OH masers. Fontani et al. (2010) recently made a survey of this maser line toward 88 high-mass protostellar candidates and obtained a detection rate of 31% at a similar detection limit to this study. The sources in their sample are divided into two groups: *low* and *high*. The sources in the *high* group may be at later evolutionary stages than those in the *low* group. The *high* group has a detection rate about three times higher than the low group: 48% versus 17%. Haschick et al. (1990) surveyed 50 star-forming regions, the vast majority of which are ultracompact and compact H II regions. They detected maser emission in 50% of them with one order of magnitude higher flux limit than

Table 8
Observed H_2O Maser Line Intensities toward the NGC 7129 Region

Observing Date	Line Number[a]	v_{LSR} (km s^{-1})	NGC 7129 FIRS2 F_{peak} (Jy)	V373 Cep F_{peak} (Jy)	V361 Cep F_{peak} (Jy)	V361 Cep Theoretical Estimation (Jy)
2010 May 8	1	−21.80	<1.33	3.44	<2.33	0.62 ± 0.10
	2	−18.43	<1.33	10.66	4.55	1.92 ± 0.32
	3	−16.54	<1.33	12.54	2.44	2.26 ± 0.38
	4	−15.06	<1.33	9.32	<2.33	1.68 ± 0.28
	5	−12.53	<1.33	55.28	9.99	9.96 ± 1.67
	6	−11.27	188.48	<2.55	11.43	7.31 ± 0.30
	7	−9.59	<1.33	50.84	9.43	9.16 ± 1.54
	8	−7.48	87.13	<2.55	5.11	3.38 ± 0.14
	9	−6.21	<1.33	9.43	5.33	1.70 ± 0.28
	10	−5.37	24.42	<2.55	3.33	0.95 ± 0.04
2010 Oct 20	1	−15.27	<1.78	16.43	<2.44	2.96 ± 0.50
	2	−13.38	<1.78	24.42	<2.44	4.40 ± 0.73
	3	−11.48	288.93	24.31	12.21	11.21 ± 0.46
	4	−9.59	<1.78	96.35	16.54	17.36 ± 2.91
	5	−7.90	1814.96	118.22	77.59	70.39 ± 2.92
	6	−4.95	103.12	6.99	4.66	4.00 ± 0.17
2010 Dec 2	1	−16.54	<2.22	14.32	<2.11	2.58 ± 0.43
	2	−14.22	<2.22	24.75	3.88	4.46 ± 0.75
	3	−11.48	110.00	46.95	8.32	4.27 ± 0.02
	4	−9.59	<2.22	58.61	7.66	10.56 ± 1.77
	5	−7.90	900.99	60.83	33.30	34.94 ± 1.45
	6	−5.16	37.07	4.11	<2.11	1.44 ± 0.06
	7	−1.37	<2.22	5.22	<2.11	0.94 ± 0.16

Note. [a] Numbers of each line are displayed in Figure 6.

this study. In the high-mass regime, therefore, the detection rate of 44 GHz Class I CH_3OH maser emission also increases significantly as the central (proto)stars evolve (see Voronkov et al. 2010b for 9.9 GHz Class I CH_3OH masers). This is in contrast with the HAeBe stars, for which we find a detection rate of 1% for CH_3OH masers.

Consequently, taking into account that UCHII regions are still deeply embedded in dense molecular cores, whereas low- and intermediate-mass PMS stars have already emerged as visible objects, the occurrence of both masers seems to be closely related to the circumstellar environments as well as the evolutionary stage of the central objects (see Section 4.1).

5.2. Relative Velocities of Masers with Respect to the Ambient Gas

While the details are still poorly understood, both H_2O and Class I CH_3OH masers are thought to be collisionally pumped (Elitzur et al. 1989; Cragg et al. 1992). The presence of shocks is a necessary condition to enhance the abundances of H_2O and CH_3OH molecules, favoring the formation of collisionally pumped masers. One plausible mechanism for inducing interstellar shocks is jets and outflows from YSOs. In fact, H_2O and Class I CH_3OH masers were found to be associated with jets and/or outflows in many YSOs (Felli et al. 1992; Kurtz et al. 2004; Cyganowski et al. 2009), although Class I CH_3OH maser emission can be related to expanding H II regions (Voronkov et al. 2010b).

Figure 7 displays the relative velocities of both masers with respect to the natal dense molecular cores against the bolometric luminosities of the central (proto)stars, L_{bol}. Here the peak velocities (v_{peak}) of Tables 3 and 4 are used. The

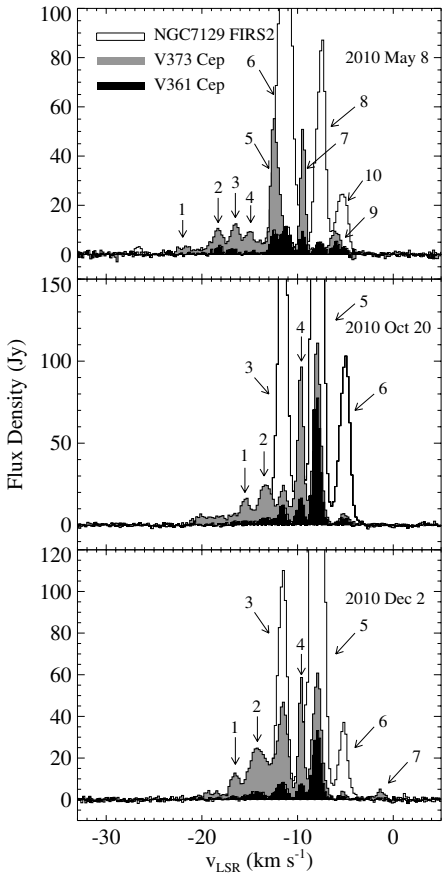

Figure 6. Spectra of the H_2O maser emission detected toward NGC 7129 FIRS2, V373 Cep, and V361 Cep.

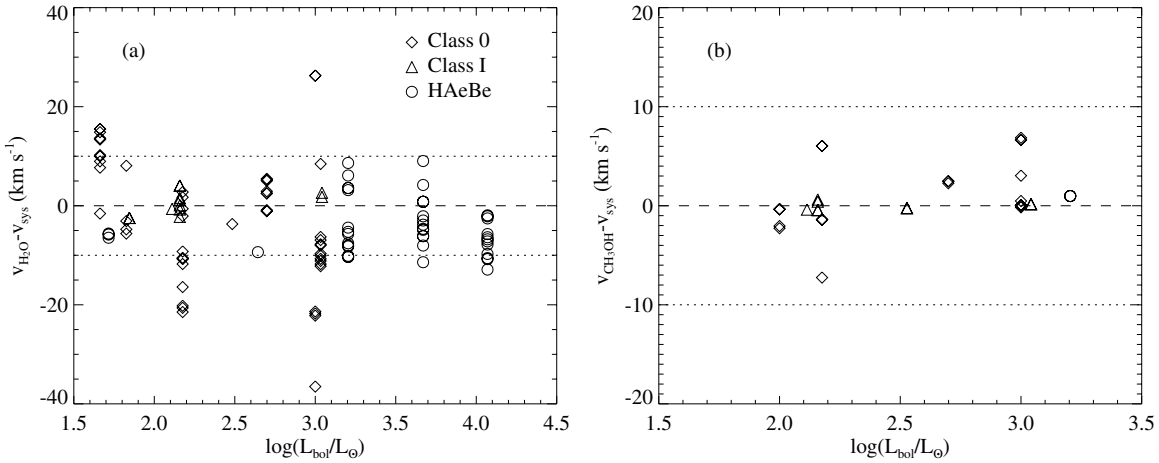

Figure 7. Relative velocity with respect to the associated molecular gas vs. the bolometric luminosity of the central (proto)star for (a) H_2O maser lines and (b) 44 GHz Class I CH_3OH maser lines. Diamonds, triangles, and circles represent data for Class 0, Class I, and HAeBe sources, respectively. The dashed lines represent the zero velocity difference and the dotted lines indicate 10 km s^{-1} of velocity difference. This figure does not include data of IRAS 20050+2720 MMS1, which shows an exceptionally large velocity difference, −90 km s^{-1} in the first observation and −93 km s^{-1} in the second observation.

Table 9
Systemic Velocities and Maser Luminosities of Detected Sources

Source	v_{sys} (km s^{-1})	Transition	Ref.	L_{H_2O}[a] ($L_\odot$)	L_{CH_3OH}[a] ($L_\odot$)
CB 3	−38.8	$N_2H^+(J = 1–0)$	1	$[1.5, 3.5, 1.3] \times 10^{-6}$	$[7.9, 8.2, 8.3] \times 10^{-6}$
IRAS 00338+6312	−17.7	$CS(J = 2–1)$	2	$[4.6, 2.6, \cdots] \times 10^{-8}$	$[1.1, 1.3, 1.5] \times 10^{-7}$
OMC3 MMS9	+11.6	$N_2H^+(J = 1–0)$	3	...	$[2.2, \cdots, \cdots] \times 10^{-8}$
OMC2 FIR4	+11.3	$N_2H^+(J = 1–0)$	3	...	$[8.2, 9.3, 9.5] \times 10^{-7}$
IRAS 05338−0624	+7.1	$NH_3(1, 1)$	4	$[2.7, 2.9, 2.3] \times 10^{-7}$	$[3.0, \cdots, 4.9] \times 10^{-8}$
IRAS 05338−0647	+9.1	$CS(J = 3–2)$	5	$[4.7, 6.5, 3.6] \times 10^{-7}$	...
IRAS 05375−0731	+5.3	$NH_3(1, 1)$	4	$[0.24, 0.61, 5.2] \times 10^{-7}$	...
IRAS 06571−0441	+25.9	$CS(J = 2–1)$	2	$[3.2, \cdots, \cdots] \times 10^{-7}$	...
Serpens FIRS1	+8.3	$NH_3(1, 1)$	6	$[3.2, 1.1, 0.98] \times 10^{-7}$	...
HH 165	+31.5	$^{12}CO(J = 3–2)$	7	$[2.9, 5.4, 4.4] \times 10^{-8}$	...
IRAS 20050+2720 MMS1	+5.9	$NH_3(1, 1)$	4	$[1.8, 1.6, 0.49] \times 10^{-7}$	...
V1318 CygS	+7.9	$^{12}CO(J = 2–1)$	8	$[6.5, 4.9, 3.5] \times 10^{-6}$	$[1.2, 1.2, 1.3] \times 10^{-6}$
S106 FIR	−1.6	$NH_3(1, 1)$	4	$[6.4, 3.7, 1.1] \times 10^{-7}$	...
V645 Cyg	−44.1	$NH_3(1, 1)$	9	$[5.2, 6.2, 5.6] \times 10^{-5}$	...
IRAS 21391+5802	+0.5	$NH_3(1, 1)$	4	$[7.6, 7.7, 3.7] \times 10^{-7}$	$[3.8, 3.3, 2.9] \times 10^{-7}$
NGC 7129 FIRS2	−10.4	$NH_3(1, 1)$	9	$[1.4, 6.9, 3.8] \times 10^{-5}$	$[2.2, 3.3, 2.6] \times 10^{-7}$
V373 Cep	−10.4	$NH_3(1, 1)$	9	$[5.5, 4.8, 3.8] \times 10^{-6}$	...
IRAS 22176+6303	−8.1	$^{12}CO(J = 1–0)$	10	...	$[3.0, 3.1, 2.8] \times 10^{-7}$
IRAS 23011+6126	−11.0	$NH_3(1, 1)$	4	...	$[0.58, 1.1, 0.47] \times 10^{-7}$
IRAS 23037+6213	−9.8	$CS(J = 2–1)$	11	$[7.8, \cdots, \cdots] \times 10^{-8}$	...

Note. [a] Numbers in the parentheses represent the maser luminosities in each observation epoch.
References. (1) De Vries et al. 2002; (2) Bronfman et al. 1996; (3) Tatematsu et al. 2008; (4) de Gregorio-Monsalvo et al. 2006; (5) Viti et al. 2006; (6)Ungerechts & Güsten 1984; (7) Dent & Aspin 1992; (8) Palla et al. 1995; (9) Scappini & Codella 1996; (10) Yang et al. 2002; (11)Williams & Myers 1999.

molecular gas velocities are collected from the literature and are presented in Table 9 with the references. In Figure 7(a), the velocity difference between H_2O masers and the associated molecular gas has an average of 9.3 km s^{-1} and a median of 6.5 km s^{-1}. While these values are much smaller than the typical shock velocity (∼100 km s^{-1}) suggested by theoretical models (Elitzur et al. 1989), they are similar to the observed velocities of molecular outflows, which range from a few km s^{-1} to about 20 km s^{-1} (e.g., Kim & Kurtz 2006), as well as the velocity differences obtained by the previous H_2O maser surveys, ∼5–10 km s^{-1} (Churchwell et al. 1990; Palla et al. 1991; Kurtz & Hofner 2005; Urquhart et al. 2009). In addition, large relative velocities (>10 km s^{-1}) are mostly confined to objects in the earliest, Class 0, evolutionary stage. This is probably because outflows are strongest during the Class 0 stage and are weakened as the central (proto)stars evolve (Bontemps et al. 1996; Arce & Sargent 2006). On the other hand, CH_3OH masers usually show much smaller relative velocities than H_2O masers. In Figure 7(b), their relative velocities are clustered around 0 km s^{-1} and do not deviate more than 10 km s^{-1} (see also Bachiller et al. 1990; Fontani et al. 2010). Furthermore, the sources with relative velocities >1 km s^{-1} are all Class 0 objects. This might also be accounted for with the strength of outflows, as for H_2O masers. However, it is worth noting that there is at least one example of a Class I CH_3OH maser that shows a significant velocity offset (∼30 km s^{-1}) from the associated molecular gas (Voronkov et al. 2010a).

Previous high-resolution studies have shown that H_2O masers are usually located closer to the central (proto)stars than Class I CH_3OH masers (e.g., Kurtz et al. 2004). It is thus widely believed that H_2O maser emission originates from the inner parts of outflows while Class I CH_3OH maser emission comes from the interacting interface of outflows with the ambient gas. This view is supported by theoretical studies showing that H_2O masers form in warm ($\sim$500 K), very dense ($\sim 10^9$ cm^{-3}) gas behind high-velocity shocks while Class I CH_3OH masers can arise in much less dense ($\sim 10^5$ cm^{-3}) post-shock gas at considerably lower ($\sim$100 K) temperatures (Elitzur et al. 1989; Cragg et al. 1992). Moreover, the CH_3OH molecule can survive sputtering or desorption of grain mantles only at low (<10 km s^{-1}) shock velocities (Garay et al. 2002). Our study cannot distinguish different spatial distributions of H_2O and CH_3OH masers owing to low angular resolution. Nevertheless, our spectroscopic results indicate that the emitting regions of the two masers are different. Our results support the previous suggestions that H_2O maser emission originates from the base of an outflow whereas Class I CH_3OH maser emission arises from the interaction region of the outflow with the ambient gas. Figure 7 also shows that no correlation exists between the relative velocities of either maser and the bolometric luminosities of the central objects.

5.3. Variability of Masers

It is well known that the intensity and shape of H_2O maser line emission can vary considerably on timescales of weeks to years (Tofani et al. 1995; Claussen et al. 1996; Furuya et al. 2003; Brand et al. 2003; Breen et al. 2010). Although our observations are confined to three epochs within a year, Figure 1 shows notable changes in H_2O maser line intensity and velocity. In particular, the integrated line intensity of Serpens FIRS1 ($v_{\rm LSR} \simeq +23$ km s^{-1}) decreased by a factor of 70 in seven months, and that of NGC 7129 FIRS2 ($v_{\rm LSR} \simeq -8$ km s^{-1}) increased by a factor of 30 in five months. Moreover, the appearance of new maser lines (CB 3, Serpens FIRS1, IRAS 20050+2720 MMS1, and S106 FIR) and disappearance of others (IRAS 00338+6312, IRAS 05375−0731, IRAS 06571−0441, IRAS 20050+2720 MMS1, and IRAS 23037+6213) is further evidence of variability.

Despite the short lifetime of the H_2O maser lines and the blending of several velocity components, we could find line-of-sight velocity drifts of H_2O maser lines in half of the 16 maser-detected sources: CB 3, IRAS 00338+6312, HH 165, IRAS 20050+2720 MMS1, V1318 CygS, V645 Cyg, IRAS 21391+5802, and NGC 7129 FIRS2. The velocity gradients of these sources except one are 0.5–2.2 km s^{-1} yr^{-1}, which are similar to other published results, e.g., 1.5 km s^{-1} yr^{-1} (Hunter et al. 1994), 1.2 km s^{-1} yr^{-1} (Tofani et al. 1995), and <1.8 km s^{-1} yr^{-1} (Brand et al. 2003). The exception is IRAS 20050+2720 MMS1, which shows an extremely large velocity gradient of 6.0 km s^{-1} yr^{-1}. Because of the coarse sampling and the low spatial resolution of our observations, however, we cannot exclude the possibility that the velocity variation was caused by different maser features, i.e., the disappearance of one maser feature and the appearance of another at a similar position.

On the other hand, the variability of the 44 GHz CH_3OH maser has not been well established. By comparing their observational results with the published data, Kurtz et al. (2004) could not find CH_3OH maser variability except for two objects in their sample. Kalenskii et al. (2010) presented observational results of three low-mass YSOs at three epochs with two-year intervals. Their spectra do not reveal any significant variability. Our results exhibit only small variation in the CH_3OH maser line intensity, shape, and velocity over a one-year interval (Figure 2). The integrated intensities are changed by $\lesssim$50% except for IRAS 05338-0624 and IRAS 23011+6126, which have poor signal-to-noise ratios.

Tofani et al. (1995) found from the H_2O maser line observations of 22 YSOs with the VLA and Medicina 32 m radio telescopes that variability of the maser emission tends to be more pronounced for maser spots closer to the central star and for those with larger relative velocity with respect to the molecular gas. Thus, these different variability behaviors of H_2O and 44 GHz CH_3OH masers may also be connected with different emitting environments (see Section 5.2).

5.4. The Relationship of Maser Luminosity with Bolometric Luminosity

The isotropic maser luminosity can be calculated from the observed line integral using the following equations:

$$L_{\rm H_2O} = 4\pi d^2 \frac{\nu}{c} \int F_\nu d\nu = 5.79 \times 10^{-9}\, L_\odot \times \left(\frac{d}{500\,{\rm pc}}\right)^2 \left(\frac{\int F_\nu d\nu}{1\,{\rm Jy\,km\,s^{-1}}}\right) \left(\frac{\eta_a}{0.72}\right)^{-1} \quad (1)$$

and

$$L_{\rm CH_3OH} = 1.15 \times 10^{-8}\, L_\odot \left(\frac{d}{500\,{\rm pc}}\right)^2 \left(\frac{\int F_\nu d\nu}{1\,{\rm Jy\,km\,s^{-1}}}\right) \left(\frac{\eta_a}{0.69}\right)^{-1}. \quad (2)$$

Here d is the distance to the source, η_a is the antenna efficiency at the observed frequency ν, and A_p is the geometric area of the antenna aperture plane. Table 9 presents the derived isotropic maser luminosities using the distances of the central objects presented in Table 1. For sources with multiple maser lines, the maser luminosity is calculated as the sum of all the individual lines.

Figure 8(a) plots $L_{\rm H_2O}$ against $L_{\rm bol}$. There is a good correlation between the two. A linear least-squares fit to our observed data points results in $L_{\rm H_2O} = 1.71 \times 10^{-9} (L_{\rm bol})^{0.97}$ with a correlation coefficient (ρ) of 0.72. Figure 8(b) exhibits a plot of $L_{\rm CH_3OH}$ versus $L_{\rm bol}$. The fitted relation is $L_{\rm CH_3OH} = 1.71 \times 10^{-10} (L_{\rm bol})^{1.22}$ with $\rho = 0.71$. The slope of 1.22 is steeper than that for the H_2O masers. It is expected from the two relations that there may be a correlation between $L_{\rm H_2O}$ and $L_{\rm CH_3OH}$. Figure 8(c) shows the relation. A linear fit to the data points yields $L_{\rm CH_3OH} = 1.13 \times 10^{-4} (L_{\rm H_2O})^{0.42}$ ($\rho = 0.45$).

For comparison, we plot 20 H_2O maser data points of low-mass ($L_{\rm bol} < 40\,L_\odot$) YSOs and 38 H_2O and 30 CH_3OH maser data points of UCHII regions together with our data in Figure 9 (Furuya et al. 2003; W.-J. Kim et al. 2011, in preparation). The data of UCHII regions were obtained with the same telescope as in this survey. One can clearly see that the luminosities of both masers are well correlated with the bolometric luminosity. The fitted relations are $L_{\rm H_2O} = 4.10 \times 10^{-9} (L_{\rm bol})^{0.84}$ ($\rho = 0.88$) and $L_{\rm CH_3OH} = 2.89 \times 10^{-9} (L_{\rm bol})^{0.73}$ ($\rho = 0.80$), which are shown by the solid lines in Figures 9(a) and (b). Figure 9(c) shows $L_{\rm CH_3OH}$ versus $L_{\rm H_2O}$ with the fitted relation, $L_{\rm CH_3OH} = 3.44 \times 10^{-3} (L_{\rm H_2O})^{0.61}$ ($\rho = 0.73$).

Several previous studies of H_2O masers in Galactic star-forming regions have produced similar relations of $L_{\rm H_2O}$ with

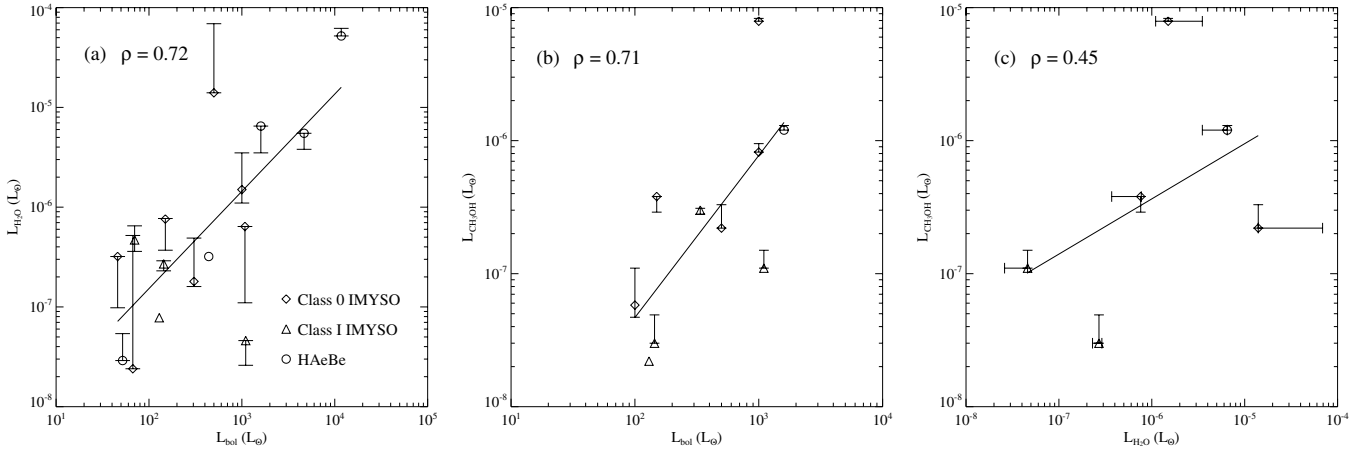

Figure 8. (a) H_2O maser luminosity vs. bolometric luminosity, (b) CH_3OH maser luminosity vs. bolometric luminosity, and (c) CH_3OH maser luminosity vs. H_2O maser luminosity. Diamonds, triangles, and circles in each panel indicate the data points of Class 0, Class I, and HAeBe sources in the first epoch, respectively. The error bars represent the variability of maser luminosity through the entire observations. In each panel, the solid line is the fitted relation to the data points and the correlation coefficient is shown at the upper left corner.

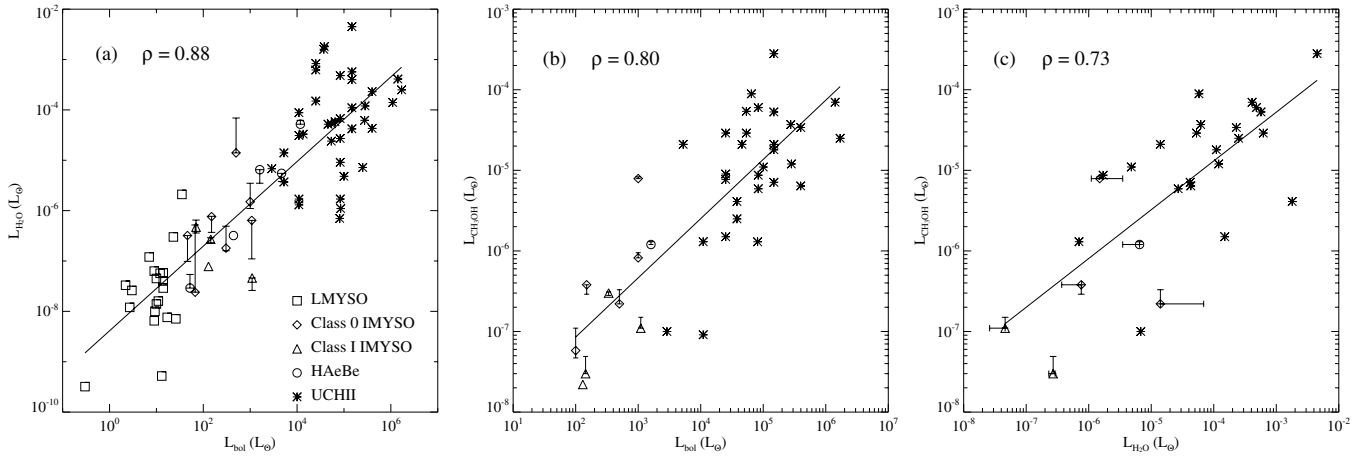

Figure 9. Same as Figure 8, but data in low- and high-mass regimes are added. Squares in panel (a) are the data points of low-mass YSOs from Furuya et al. (2003), while asterisks in all three panels represent the data points of UCHII regions from W.-J. Kim et al. (2011, in preparation). In each panel the solid line is the fitted relation to all data points.

L_{bol} (Wouterloot & Walmsley 1986; Felli et al. 1992; Brand et al. 2003; Furuya et al. 2003). Our slope agrees well with the previous values, 0.8–1.0. For a given evolutionary stage, therefore, YSOs with higher bolometric luminosities are expected to have higher H_2O maser luminosities. However, we are unaware of any study examining the L_{bol}–L_{CH_3OH} and L_{H_2O}–L_{CH_3OH} relations.

6. SUMMARY

We have carried out a multi-epoch, simultaneous 22 GHz H_2O and 44 GHz Class I CH_3OH maser line survey toward 180 IMYSOs. The main results are summarized as follows.

1. We detected H_2O masers toward 16 objects and CH_3OH masers toward 10 objects. One new H_2O maser source (HH 165) and six new CH_3OH maser sources (CB 3, IRAS 00338+6312, OMC3 MMS9, IRAS 05338−0624, V1318 CygS, and IRAS 23011+6126) were found in our survey.
2. The overall detection rates of H_2O masers and CH_3OH masers are 9% and 6%, respectively. The rates rapidly decrease as the central (proto)stars evolve. The detection rates of H_2O masers are 50%, 21%, and 3% for Class 0, Class I, and HAeBe objects, respectively. Those of CH_3OH masers for Class 0, Class I, and HAeBe objects are 36%, 21%, and 1%. In contrast, the detection rates of both masers in high-mass star-forming regions significantly increase as the central objects evolve from the protostellar to the main-sequence stage. These results indicate that the occurrence of the two masers are closely related both to the evolutionary stage of the central (proto)stars and to the circumstellar environments.
3. The relative velocities of H_2O masers with respect to the ambient molecular gas are 9.3 km s^{-1} on average, with a median difference of 6.5 km s^{-1}, whereas those of CH_3OH masers are concentrated around 0 km s^{-1}. No CH_3OH maser velocity deviates more than 10 km s^{-1} from the systemic velocity. Large relative velocities are mainly shown in the Class 0 objects: $|v_{H_2O} - v_{sys}| > 10\,km\,s^{-1}$ and $|v_{CH_3OH} - v_{sys}| > 1\,km\,s^{-1}$. This is consistent with previous suggestions that H_2O masers originate from the inner parts of outflows while Class I CH_3OH masers arise from the interacting interface of outflows with the ambient dense gas.
4. The intensities and shapes of the observed H_2O maser lines were quite variable. Half of the maser-detected sources show velocity drifts. The integrated line intensities varied by up to two orders of magnitude. In contrast, the observed

CH_3OH lines do not reveal any significant variability in intensity, shape, or velocity. The line integrals were maintained within ∼50% over the observations. These different variability behaviors of the two masers may be connected with different emitting environments.

5. The isotropic luminosities of both masers are well correlated with the bolometric luminosities of the central objects. The linear fits result in $L_{H_2O} = 1.71 \times 10^{-9}(L_{bol})^{0.97}$ and $L_{CH_3OH} = 1.71 \times 10^{-10}(L_{bol})^{1.22}$ when only IMYSO data in this survey were considered, while those yield $L_{H_2O} = 4.10 \times 10^{-9}(L_{bol})^{0.84}$ and $L_{CH_3OH} = 2.89 \times 10^{-9}(L_{bol})^{0.73}$, after the data points of low- and high-mass regimes are added.

We are very grateful to Stan Kurtz for carefully reading the manuscript and for many helpful comments. We also thank the anonymous referee for constructive comments.

REFERENCES

Alonso-Albi, T., Fuente, A., Bachiller, R., et al. 2009, A&A, 497, 117
Alonso-Albi, T., Fuente, A., Crimier, N., et al. 2010, A&A, 518, A52
Arce, H. G., & Sargent, A. I. 2006, ApJ, 646, 1070
Bachiller, R., Fuente, A., & Tafalla, M. 1995, ApJ, 445, L51
Bachiller, R., Menten, K. M., Gómez-González, J., & Barcia, A. 1990, A&A, 240, 116
Beltrán, M. T., Estalella, R., Anglada, G., Rodríguez, L. F., & Torrelles, J. M. 2001, AJ, 121, 1556
Bontemps, S., André, P., Terebey, S., & Cabrit, S. 1996, A&A, 311, 858
Brand, J., Cesaroni, R., Comoretto, G., et al. 2003, A&A, 407, 573
Breen, S. L., Caswell, J. L., Ellingsen, S. P., & Phillips, C. J. 2010, MNRAS, 406, 1487
Bronfman, L., Nyman, L.-A., & May, J. 1996, A&AS, 115, 81
Caswell, J. L., & Breen, S. L. 2010, MNRAS, 407, 2599
Cesarsky, C. J., Cesarsky, D. A., Churchwell, E., & Lequeux, J. 1978, A&A, 68, 33
Chen, X., Launhardt, R., & Henning, T. 2009, ApJ, 691, 1729
Chini, R., Ward-Thompson, D., Kirk, J. M., et al. 2001, A&A, 369, 155
Churchwell, E., Walmsley, C. M., & Cesaroni, R. 1990, A&AS, 83, 119
Claussen, M. J., Marvel, K. B., Wootten, A., & Wilking, B. A. 1998, ApJ, 507, L79
Claussen, M. J., Wilking, B. A., Benson, P. J., et al. 1996, ApJS, 106, 111
Connelley, M. S., Reipurth, B., & Tokunaga, A. T. 2007, AJ, 133, 1528
Connelley, M. S., Reipurth, B., & Tokunaga, A. T. 2008, AJ, 135, 2496
Cragg, D. M., Johns, K. P., Godfrey, P. D., & Brown, R. D. 1992, MNRAS, 259, 203
Cyganowski, C. J., Brogan, C. L., Hunter, T. R., & Churchwell, E. 2009, ApJ, 702, 1615
de Gregorio-Monsalvo, I., Gómez, J. F., Suárez, O., et al. 2006, ApJ, 642, 319
Dent, W. R. F., & Aspin, C. 1992, MNRAS, 259, 401
Dent, W. R. F., Matthews, H. E., & Ward-Thompson, D. 1998, MNRAS, 301, 1049
De Vries, C. H., Narayanan, G., & Snell, R. L. 2002, ApJ, 577, 798
Eiora, C., Palacios, J., & Casali, M. M. 1998, A&A, 335, 243
Eislöfell, J., Mundt, R., & Böhm, K.-H. 1994, AJ, 108, 1042
Elitzur, M., Hollenbach, D. J., & McKee, C. F. 1989, ApJ, 346, 983
Felli, M., Palagi, F., & Tofani, G. 1992, A&A, 255, 293
Fontani, F., Cesaroni, R., & Furuya, R. S. 2010, A&A, 517, A56
Froebrich, D. 2005, ApJS, 156, 169
Furuya, R. S., Kitamura, Y., Wootten, H. A., Claussen, M. J., & Kawabe, R. 2001, ApJ, 559, L143
Furuya, R. S., Kitamura, Y., Wootten, H. A., Claussen, M. J., & Kawabe, R. 2003, ApJS, 144, 71
Furuya, R. S., Kitamura, Y., Wootten, H. A., Claussen, M. J., & Kawabe, R. 2005, A&A, 438, 571
Garay, G., Mardones, D., Rodríguez, L. F., Caselli, P., & Bourke, T. L. 2002, ApJ, 567, 980
Genzel, R., & Downes, D. 1977, A&AS, 30, 145
Gregorio-Hetem, J., Lépine, J. R. D., Quast, G. R., Torres, C. A. O., & de la Reza, R. 1992, AJ, 103, 549
Han, F., Mao, R. Q., Lu, J., et al. 1998, A&AS, 127, 181
Han, S.-T., Lee, J.-W., Kang, J., et al. 2008, Int. J. Infrared Millim. Waves, 29, 69
Haschick, A. D., Menten, K. M., & Baan, W. A. 1990, ApJ, 354, 556
Hernández, J., Calvet, N., Briceño, C., Hartmann, L., & Berlind, P. 2004, AJ, 127, 1682
Hillenbrand, L. A., Meyer, M. R., Strom, S. E., & Skrutskie, M. F. 1995, AJ, 109, 280
Hirota, T., Bushimata, T., Choi, Y. K., et al. 2007, PASJ, 59, 897
Hunter, T. R., Taylor, G. B., Felli, M., & Tofani, G. 1994, A&A, 284, 215
Kalenskii, S. V., Johansson, L. E. B., Bergman, P., et al. 2010, MNRAS, 405, 613
Kim, K.-T., Byun, D.-Y., Je, D.-H., et al. 2011, J. Korean Astron. Soc., 44, 81
Kim, K.-T., & Kurtz, S. E. 2006, ApJ, 643, 978
Kurtz, S., & Hofner, P. 2005, AJ, 130, 711
Kurtz, S., Hofner, P., & Álvarez, C. V. 2004, ApJS, 155, 149
Lada, C. J., Blitz, L., Reid, M. J., & Moran, J. M. 1981, ApJ, 243, 769
Lee, S.-S., Byun, D.-Y., Oh, C. S., et al. 2011, PSAP, submitted
Malfait, K., Bogaert, E., & Waelkens, C. 1998, A&A, 331, 211
Mannings, V., & Sargent, A. I. 2000, ApJ, 529, 391
Manoj, P., Bhatt, H. C., Maheswar, G., & Muneer, S. 2006, ApJ, 653, 657
Martí, J., Rodríguez, L. F., & Torrelles, J. M. 1999, A&A, 345, L5
Marvel, K. B. 2005, AJ, 130, 2732
Menten, K. M. 1991, in ASP Conf. Ser. 16, Atoms, Ions and Molecules: New Results in Spectral Line Astrophysics, ed. A. D. Haschick & P. T. P. Ho (San Francisco, CA: ASP), 119
Montesinos, B., Eiroa, C., Mora, A., & Merín, B. 2009, A&A, 495, 901
Mora, A., Merín, B., Solano, E., et al. 2001, A&A, 378, 116
Palla, F., Brand, J., Cesaroni, R., Comoretto, G., & Felli, M. 1991, A&A, 246, 249
Palla, F., & Prusti, T. 1993, A&A, 272, 249
Palla, F., Testi, L., Hunter, T. R., et al. 1995, A&A, 293, 521
Rodriguez, L. F., Haschick, A. D., Torrelles, J. M., & Myers, P. C. 1987, A&A, 186, 319
Rodriguez, L. F., Moran, J. M., Ho, P. T. P., & Gottlieb, E. W. 1980, ApJ, 235, 845
Sandell, G., Avery, L. W., Baas, F., et al. 1999, ApJ, 519, 236
Saraceno, P., André, P., Ceccarelli, C., Griffin, M., & Molinari, S. 1996, A&A, 309, 827
Sartori, M. J., Gregorio-Hetem, J., Rodrigues, C. V., Hetem, A., Jr., & Batalha, C. 2010, AJ, 139, 27
Scappini, F., & Codella, C. 1996, MNRAS, 282, 587
Schwartz, P. R., & Buhl, D. 1975, ApJ, 201, L27
Seth, A. C., Greenhill, L. J., & Holder, B. P. 2002, ApJ, 581, 325
Sridharan, T. K., Beuther, H., Schilke, P., Menten, K. M., & Wyrowski, F. 2002, ApJ, 566, 931
Strom, S. E., Strom, K. M., Grasdalen, G. L., et al. 1985, AJ, 90, 2281
Szymczak, M., Pillai, T., & Menten, K. M. 2005, A&A, 434, 613
Tatematsu, K., Kandori, R., Umemoto, T., & Sekimoto, Y. 2008, PASJ, 60, 407
Thé, P. S., de Winter, D., & Pérez, M. R. 1994, A&AS, 104, 315
Tofani, G., Felli, M., Taylor, G. B., & Hunter, T. R. 1995, A&AS, 112, 299
Torrelles, J. M., Ho, P. T. P., Moran, J. M., Rodríguez, L. F., & Cantó, J. 1986, ApJ, 307, 787
Torres, C. A. O., Quast, G., de la Reza, R., Gregorio-Hetem, J., & Lépine, J. R. D. 1995, AJ, 109, 2146
Ungerechts, H., & Güsten, R. 1984, A&A, 131, 177
Urquhart, J. S., Hoare, M. G., Lumsden, S. L., et al. 2009, A&A, 507, 795
Val'tts, I. E., Larionov, G. M., & Bayandina, O. S. 2010, arXiv:1005.3715
Vieira, R. G., Gregorio-Hetem, J., Hetem, A., Jr., Stasińska, G., & Szczerba, R. 2011, A&A, 526, A24
Vieira, S. L. A., Corradi, W. J. B., Alencar, S. H. P., et al. 2003, AJ, 126, 2791
Viti, S., Girart, J. M., & Hatchell, J. 2006, A&A, 449, 1089
Voronkov, M. A., Caswell, J. L., Britton, T. R., et al. 2010a, MNRAS, 408, 133
Voronkov, M. A., Caswell, J. L., Ellingsen, S. P., & Sobolev, A. M. 2010b, MNRAS, 405, 2471
Waters, L. B. F. M., & Waelkens, C. 1998, ARA&A, 36, 233
Weaver, H., Williams, D. R. W., Dieter, N. H., & Lum, W. T. 1965, Nature, 208, 29
Wilking, B. A., Claussen, M. J., Benson, P. J., et al. 1994, ApJ, 431, L119
Williams, J. P., & Myers, P. C. 1999, ApJ, 511, 208
Wolf-Chase, G., Moriarty-Schieven, G., Fich, M., & Barsony, M. 2003, MNRAS, 344, 809
Wouterloot, J. G. A., & Walmsley, C. M. 1986, A&A, 168, 237
Wu, Y., Huang, M., & He, J. 1996, A&AS, 115, 283
Wu, Y., Wei, Y., Zhao, M., et al. 2004, A&A, 426, 503
Yang, J., Jiang, Z., Wang, M., Ju, B., & Wang, H. 2002, ApJS, 141, 157